



Yasir Abdul Qadir



# MULTI-COLOR HIGH-PRECISION OPTICAL POLARIMETRY OF BINARY STARS AND EXOPLANETS

Yasir Abdul Qadir

#### **University of Turku**

Faculty of Science
Department of Physics and Astronomy
Astronomy
Doctoral Programme in Exact Sciences (EXACTUS)

#### Supervised by

Doc. Andrei Berdyugin Department of Physics and Astronomy, University of Turku, Turku, Finland Prof. Juri Poutanen
Department of Physics and Astronomy,
University of Turku,
Turku, Finland

#### Reviewed by

Prof. Gražina Tautvaišienė Institute of Theoretical Physics and Astronomy, Vilnius University, Vilnius, Lithuania Dr. B-G Andersson McDonald Observatory, University of Texas, Austin, USA

#### **Opponent**

Doc. Vitaly Neustroev Space Physics & Astronomy Research Unit, University of Oulu, Oulu, Finland

The originality of this publication has been checked in accordance with the University of Turku quality assurance system using the Turnitin OriginalityCheck service.

Cover Image: Artistic impression created by the author with the assistance of OpenAI's DALL·E.

ISBN 978-952-02-0432-7 (PRINT) ISBN 978-952-02-0433-4 (PDF) ISSN 0082-7002 (PRINT) ISSN 2343-3175 (ONLINE) Painosalama, Turku, Finland, 2025

UNIVERSITY OF TURKU
Faculty of Science
Department of Physics and Astronomy
Astronomy
ABDUL QADIR, YASIR: Multi-color High-precision Optical Polarimetry of Binary Stars and Exoplanets
Doctoral dissertation, 106 pp.
Doctoral Programme in Exact Sciences (EXACTUS)
October 2025

#### **ABSTRACT**

This dissertation presents a comprehensive study of multi-wavelength optical polarimetry applied to stellar systems exhibiting variable intrinsic polarization, with a focus on close binary stars and exoplanets. Using high-precision broadband polarimetry with the DiPol-2 instrument on the remotely controlled T60 telescope, we have measured polarization variations with the phase of the orbital period in three O+O binary systems (AO Cassiopeiae (AO Cas), DH Cephei (DH Cep), and HD 165052) and the exoplanet Upsilon Andromedae b (v And b). For two binary systems, DH Cep and HD 165052, phase-locked small-amplitude polarization variability has been detected and analyzed for the very first time.

For the binary systems, we derived orbital parameters through Fourier analysis of polarization variability, obtaining inclinations and orientations of the orbital planes. Our analysis revealed symmetric distributions of scattering material consistent with Thomson scattering in circumstellar environments. We estimated interstellar polarization contributions through observations of field stars, revealing uniform dust distributions in the young open stellar cluster NGC 7380 (DH Cep), but strong non-uniformity in cluster NGC 6530 (HD 165052).

For the exoplanet  $\upsilon$  And b, we detected weak periodic signals at half the orbital period but faced challenges in orbital and physical parameters extraction due to very small amplitude of periodic variations and low signal-to-noise. Our Rayleigh-Lambert modeling yielded tentative estimates of planetary orbital parameters and geometric albedo but with large uncertainties, demonstrating difficulties in exoplanet polarimetry which requires accuracy much better than  $10^{-5}$ .

This work demonstrates polarimetry's unique ability to probe orbital geometries and scattering environments in stellar systems, while establishing the current limitations for exoplanet characterization. The research advances our understanding of binary star dynamics and circumstellar environments while outlining pathways for future high-sensitivity polarimetric studies.

KEYWORDS: observational astronomy, polarimetry, binary stars, exoplanets

TURUN YLIOPISTO
Matemaattis-luonnontieteellinen tiedekunta
Fysiikan ja tähtitieteen laitos
Tähtitiede
ABDUL QADIR, YASIR: Multi-color High-precision Optical Polarimetry of Binary Stars and Exoplanets
Väitöskirja, 106 s.
Eksaktien tieteiden tohtoriohjelma
Lokakuu 2025

#### TIIVISTELMÄ

Tässä väitöskirjassa esitetään kattava monikanavaisen optisen polarimetrisen tutkimuksen kokonaisuus tähtijärjestelmistä, jotka osoittavat muuttuvaa intrinsistä polarisaatiota. Tutkimus keskittyy erityisesti lähekkäisiin kaksoistähtiin ja eksoplaneettoihin. Käyttämällä erittäin tarkkaa laajakaistaista polarimetriaa kauko-ohjatun T60-kaukoputken DiPol-2 -instrumentilla mitattiin polarisaation vaihtelua kiertoradan vaiheen funktiona kolmessa O+O-tyypin kaksoistähtijärjestelmässä (AO Cassiopeiae (AO Cas), DH Cephei (DH Cep) ja HD 165052) sekä eksoplaneetalla Upsilon Andromedae b ( $\upsilon$  And b). Kahdessa kaksoistähtijärjestelmässä, DH Cep ja HD 165052, havaittiin ja analysoitiin ensimmäistä kertaa vaiheeseen sidottua pienen amplitudin polarisaatiovaihtelua.

Kaksoistähtijärjestelmissä kiertoradan parametrit mitattiin polarisaation vaihtelun Fourier-analyysin Fourier-analyysilla, josta saatiin tietoa kiertoratojen inklinaatioista ja suunnista. Analyysi osoitti sirontamateriaalin symmetrisen jakauman, mikä on johdonmukaista Thomson-sironnan kanssa tähtiä ympäröivissä ympäristöissä. Tähtikenttien havaintojen perusteella arvioitiin myös tähtienvälinen polarisaatio. NGC 7380 -tähtijoukossa (DH Cep) havaittiin tasainen pölyjakauma, kun taas NGC 6530 -joukossa (HD 165052) pöly oli jakautunut epätasaisesti.

Eksoplaneetalla  $\upsilon$  And b havaittiin heikkoja periodisia signaaleja, joiden jakso vastaa puolta kiertoradasta. Kiertoradan ja planeetan parametrien määrittämistä vaikeutti kuitenkin vaihtelun erittäin pieni amplitudi ja alhainen signaali-kohinasuhde. Rayleigh-Lambert-mallinnuksen avulla saatiin alustavia arvioita kiertoradan parametreista ja geometristä albedosta, mutta epävarmuudet jäivät suuriksi. Tämä osoittaa, kuinka haastavaa eksoplaneettojen polarimetrinen tutkimus on, sillä se vaatii paljon parempaa tarkkuutta kuin  $10^{-5}$ .

Tämä työ osoittaa polarimetrian ainutlaatuisen kyvyn tutkia kiertoratojen geometrioita ja sirontaympäristöjä tähtijärjestelmissä sekä tuo esiin nykyiset rajoitukset eksoplaneettojen karakterisoinnissa. Tämä tutkimus syventää ymmärrystämme kaksoistähtien dynamiikasta ja tähteä ympäröivistä ympäristöistä sekä osoittaa suuntaviivoja tuleville erittäin herkille polarimetrisille tutkimuksille.

ASIASANAT: havaintotähtitiede, polarimetria, kaksoistähdet, eksoplaneetat

## Acknowledgements

I would like to express my deepest and most heartfelt gratitude to my supervisor, Doc. Andrei Berdyugin, whose guidance, mentorship, and unwavering support have been truly invaluable throughout my entire PhD journey. His expertise in polarimetric observations and his profound understanding of the subject matter have shaped my research and its outcomes in ways I could not have imagined. Doc. Berdyugin's patience, insightful advice, and constant encouragement at every stage of this research have been a cornerstone of my academic development. I am incredibly grateful for the trust he placed in me, and for his ability to always provide direction even in the most challenging moments of my work.

I am indebted to the director of my research program and my second supervisor, Prof. Juri Poutanen, whose vast knowledge and meticulous attention to detail have significantly enriched the quality of my work. His ability to approach complex scientific problems with clarity and precision has been an ongoing source of inspiration. Prof. Poutanen's thoughtful feedback and constructive criticism, which always came with the goal of enhancing the scientific rigor and presentation of my thesis, were instrumental in refining my research. I greatly appreciate the time and effort he dedicated to reviewing my work, ensuring that it met the highest academic standards.

A special note of thanks goes to Prof. Vilppu Piirola and Prof. Svetlana Berdyugina, who have overseen my work with great care and provided invaluable perspectives that have enriched my research. Their expertise in stellar polarimetry, combined with their ability to offer constructive feedback, has been instrumental in shaping my analysis and interpretations. I particularly appreciate their constant encouragement, which has been a great source of motivation, as well as the trust they placed in my abilities throughout my work. Their guidance has had a lasting impact on my academic growth.

I am fortunate to have received guidance and support from my senior colleagues, Vadim Kravtsov, Dr. Ilia Kosenkov, and Dr. Tuomo Salmi. Their insights, thoughtful discussions, and willingness to share their extensive knowledge were indispensable in navigating both the technical and theoretical challenges of this research. The collaborative environment they fostered, characterized by open communication and mutual respect, greatly contributed to my professional development. Their support extended beyond just scientific matters, providing a motivating and stimulating environment that made this journey both productive and enjoyable.

I would also like to thank the Finnish Academy of Science and Letters Väisälä Foundation for their generous financial support. This funding allowed me to focus on my research and pursue my academic goals without the added concern of financial limitations. Their contribution has been pivotal in enabling the completion of this work.

I extend my sincere appreciation to all my colleagues and collaborators at Tuorla Observatory and the University of Turku. The academic environment there has been a source of continuous inspiration throughout my doctoral studies. I am grateful for the stimulating discussions, collaboration on various projects, and the encouragement I received from everyone in the department. It was a privilege to be part of such a vibrant and intellectually stimulating community.

Finally, I am deeply thankful to my family and friends for their unwavering support, love, and understanding throughout this journey. Their constant encouragement, belief in my work, and presence in my life have been a source of strength and motivation. The balance they provided through shared experiences, conversations, and moments of respite played a crucial role in helping me maintain focus and perseverance. Without them, this research work would not have been possible.

10 March 2025 Yasir Abdul Qadir

# **Table of Contents**

A	cknowl	ledgements	6
Ta	ble of	Contents	8
A	bbrevia	ations	10
Li	st of O	Original Publications	11
Li	st of O	Other Publications	12
1	Introd	duction	13
2		retical Background of Polarization, Polarimetry of Bi-Stars, and Stars Hosting Exoplanets	18
	2.1	Polarization of Electromagnetic Waves	18
	2.2	Stokes Parameters	19
	2.3	Polarization in Binary Star Systems	22
	2.4	Thomson Scattering in Binary Star Systems	23
	2.5	Star Cluster Polarization	24
	2.6	Polarization by Exoplanets	26
	2.7	Rayleigh Scattering in Star-Exoplanet Systems	27
3	Polari	imetric Instruments and Observations	28
	3.1	Polarimetric Instrumentation	29
		3.1.1 T60 Telescope	29
		3.1.2 DiPol-2 Polarimeter	30
	3.2	Polarimetric Observations	33
	3.3	Data Reduction	33
		3.3.1 Intrinsic Polarization	35
		3.3.2 Interstellar Polarization	35
		3.3.3 Instrumental Polarization	36
4		imetry of Binary Stars	38
	4.1	Period Search	38

	4.2 BME Method								39				
	4.3 Mass-Loss Rate								46				
	4.4 Summary of Publications								47				
		4.4.1	Paper I – F try of early										ł 47
		4.4.2	Paper II – H try of early system in t	-type b	inaries	s IV.	The	DH (	Сер	hei	bina	ary	48
		4.4.3	Paper III – try of early	High-pr	ecisio	n bro	adba	ınd li	nea	r pc	olari	me-	40
			165052 in	Open C	luster	NGC	653	30 .					48
5	Polari	metry o	of Exoplar	net $v$ A	nd b								50
	5.1	_	bservations										50
	5.2		Search										52
	5.3	RL App	roximation										53
	5.4	Results	and Discus	ssion .									55
6	Concl	usions											58
List of References						61							
O <sub>I</sub>	Original Publications							60					

## **Abbreviations**

AO Cas AO Cassiopeiae AS Eri AS Eridani

BME Brown McLean Emslie CCD Charge-Coupled Device

DH Cep DH Cephei

DiPol-2 Double Image Polarimeter - 2

FAP False Alarm Probability

Her X-1 Hercules X-1

ISP Interstellar Polarization

LS Lomb-Scargle
PA Polarization Angle
PD Polarization Degree
PPM Parts Per Million
PZ Gem PZ Geminorum
RZ Cas RZ Cassiopeiae

RAT Radiative Alignment Torque

RV Radial Velocity T60 Tohoku 60

v And Upsilon (v) Andromedae

au Boö Tau ( au) Boötis

# List of Original Publications

This dissertation is based on the following original publications:

- I Abdul Qadir, Y., Berdyugin, A. V., Piirola, V., Sakanoi, T., Kagitani, M. High-precision broadband linear polarimetry of early-type binaries. III. AO Cassiopeiae revisited. *A&A*, 670, A176 (2023).
- II Abdul Qadir, Y., Berdyugin, A. V., Piirola, V., Sakanoi, T., and Kagitani, M. High-precision broadband linear polarimetry of early-type binaries. IV. The DH Cephei binary system in the open cluster of NGC 7380. *A&A*, 677, A75 (2023).
- III *Abdul Qadir, Y.*, Berdyugin, A. V., Piirola, V., Sakanoi, T., Kagitani, M., and Berdyugina, S. V. High-precision broadband linear polarimetry of early-type binaries. V. The binary system HD 165052 in open cluster NGC 6530. *A&A*, 697, A133 (2025).

# List of publications not included in the thesis

This dissertation does not include the following publications of the author:

- Kravtsov, V., Berdyugin, A. V., Kosenkov I., Veledina A., Piirola, V., *Abdul Qadir, Y.*, Berdyugina, S. V., Sakanoi, T., Kagitani, M., and Poutanen, J. Optical polarization signatures of black hole X-ray binaries. *MNRAS*, 514, 2479–2487 (2022).
- A-thano, N., Awiphan, S., Kerins, E., Priyadarshi, A., McDonald, I., Jiang, I.-G., Joshi, Y. C., Yang, F., Janiak, I., Munsaket, P., *Abdul Qadir, Y.*, Rattanamala, R., Tasuya, O., Boonsoy, E., Sanguansak, N., Rattanasai, R., Padjaroen, T., Komonjinda, S., Pichadee, S., Sudsap, A., Chandaiam, S., Choonhakit, B., Wutsang, S., and Dhillon, V. S. The Transit Timing and Transmission Spectrum of Hot Jupiter WASP-43 b from a decade of multi-band transit follow-up observations. *ApJ*, xxx, xxx (2025).
- A-thano, N., Awiphan, S., Kerins, E., Priyadarshi, A., McDonald, I., Tasuya, O., Rattanamala, R., Jiang, I.-G., Joshi, Y. C., Yang, F., Janiak, I., Munsaket, P., *Abdul Qadir, Y.*, Chandaiam, S., Choonhakit, B., Wutsang, S., and Dhillon, V. S. Investigation of Transit Timing and an Optical Transmission Spectrum of the Hot Jupiter WASP-11 b. *ApJ*, xxx, xxx (2025).

The original publications have been reproduced with the permission of the copyright holders.

## 1 Introduction

Light polarization, first discovered in 1808 by the French physicist Étienne-Louis Malus, has become one of the most powerful diagnostic tools in astronomy for probing the physical conditions, geometries, and interactions within astrophysical environments (Hiltner, 1947, 1949; Hall, 1949; Chandrasekhar, 1960). When light passes through or is scattered by interstellar dust grains, gas clouds, circumstellar material, or planetary atmospheres, these interactions can induce linear polarization, i.e., aligning the electric field vectors of the light in a preferred direction rather than at random (Serkowski et al., 1975; Andersson et al., 2015). This polarization reveals crucial information about the composition, alignment, and spatial distribution of matter, often uncovering structures and processes that remain hidden to conventional photometry or spectroscopy (Serkowski et al., 1975; Clarke, 2010).

Astronomical polarization is inherently partial, regardless of wavelength or mechanism, because only a fraction of the light is scattered, absorbed, or aligned in a preferred direction, while the remainder remains unpolarized. At radio wavelengths, synchrotron emission from relativistic electrons spiralling in magnetic fields can nevertheless produce relatively high levels of polarization, often reaching tens of percent in compact sources (e.g., Saikia and Salter, 1988). At shorter wavelengths, spectral-line polarization can be used to probe magnetic fields through the Zeeman and Hanle effects (Harrington, 1970; Leroy, 1990), while light scattering in continuum by dust grains, free electrons, or planetary atmospheres typically yields much lower values. Together, continuum and spectral-line polarimetry provide complementary diagnostics of the geometry of light-scattering material and magnetic structure. However, this work focuses specifically on optical continuum linear polarization in binary star systems and exoplanets, where the expected signals are comparatively modest or very low.

In the optical and near-infrared, interstellar dust typically produces a few percent polarization (Serkowski et al., 1975; Andersson et al., 2015). Light scattering in hot-star envelopes or circumstellar disks usually yields polarization below 1–2% (Brown et al., 1978; Abdul Qadir et al., 2023a,b, 2025). Expected exoplanetary polarization signals are much weaker, at the level of a few parts per million (Seager et al., 2000; Berdyugina et al., 2008). By contrast, X-ray and gamma-ray polarization can be substantially higher, offering unique insights into emission mechanisms and magnetic geometries in extreme environments near accreting black holes and

neutron stars (e.g., Poutanen et al., 2023; Forsblom et al., 2024; Kole et al., 2023). A clear understanding of this broad polarization landscape is essential for placing optical measurements in the context of the field of research and designing high-precision polarimetric instrumentation.

The first observational evidence of starlight polarization emerged in the mid-20th century, when Hiltner (1947, 1949) conducted measurements motivated by Chandrasekhar's prediction (Chandrasekhar, 1946) that hot stars in eclipsing binaries could exhibit polarization if symmetry in the Thomson-scattering envelopes was broken by the presence of a companion. Hiltner's observations revealed that the polarization position angles were systematically aligned with the Galactic plane, indicating that the measured polarization originated in the interstellar medium rather than in the stellar environment. No significant time-dependent polarization was detected in individual stars, consistent with the small fraction of intrinsic polarization discussed above.

Systematic polarimetric studies of binary star systems soon followed, as astronomers recognized that orbital motion within these systems could induce measurable, phase-dependent polarization variations (Hiltner, 1956; Coyne and Gehrels, 1966; Poeckert and Marlborough, 1976; Brown et al., 1978; McLean, 1979). One of the earliest comprehensive investigations of binary systems, including AO Cassiopeiae (AO Cas),  $\sigma$  Orionis E, and Cygnus X-1 was carried out by Rudy and Kemp (1976) and re-analyzed by Brown et al. (1978) who demonstrated how phase-locked polarization variations are directly linked to the distribution of light scattering material and orbital geometry of the system. Their work highlighted the power of polarimetry as a tool for probing circumstellar environments of binary stars and deriving their orbital parameters, such as orbit inclination, orientation, and direction of circumvention.

Polarimetric studies can also serve as a powerful tool for investigating interstellar dust and its distribution in star forming regions or star clusters (McMillan, 1976; Axon and Ellis, 1976; Goodman et al., 1990; Menard and Bastien, 1992; Abdul Qadir et al., 2023b, 2025). Dust grains aligned by the local Galactic magnetic field polarize the light emitted by cluster stars, and by observing multiple stars in a cluster one can map polarization patterns across a cluster, tracing dust density and magnetic field geometry (McMillan, 1976; Abdul Qadir et al., 2023b, 2025). Significant variations in polarization magnitude and direction indicate non-uniform dust distribution and tangled magnetic field geometry, which points to clumps, voids, or asymmetries, while uniform polarization suggests a smoother, more evolved dust environment (McMillan, 1976; Abdul Qadir et al., 2023b, 2025).

A complete interpretation of such polarization patterns requires consideration of modern grain alignment theory, specifically radiative alignment torques (RATs) (Dolginov and Mitrofanov, 1976; Lazarian and Hoang, 2007; Andersson et al., 2015). RAT theory predicts that the efficiency of grain alignment depends on grain size dis-

tribution and mineralogy, as well as on the intensity and spectrum of the local radiation field. Thus, the observed ISM polarization in star-forming regions not only traces magnetic field geometry but also carries information about the dust population and its radiative environment. One of the earliest systematic polarimetric surveys of star clusters, conducted on the open cluster NGC 7380 by McMillan (1976) and later repeated by Abdul Qadir et al. (2023b), demonstrated that polarization patterns can effectively reveal interstellar dust distribution in stellar cluster environments.

Early-type binary star systems, such as O+O binaries composed of two massive O-type stars in close gravitational interaction, are particularly compelling for studying polarization due to their intense radiation fields and dynamic interactions (Rudy and Kemp, 1976). These systems are characterized by phenomena such as tidal distortions, mass transfer and mass-loss due to stellar winds, which give rise to variable orbital phase locked polarization due to electron scattering (see (Berdyugin et al., 2016; Abdul Qadir et al., 2023a,b, 2025). Chandrasekhar (1946) provided the first theoretical treatment of electron scattering and its role in producing polarized light, which laid the foundation for modern polarimetric studies of circumstellar environments of the hot stars. In such environments, polarization arises primarily from the scattering of photons off free electrons, which are present in hot ionized material ejected through stellar winds or mass transfer (Shakhovskoi, 1965; Brown and McLean, 1977). This makes O+O binaries ideal laboratories for probing orbital parameters, mass-loss rates, and the geometry of their environments.

Polarization variability across the orbital phase of a binary star system can help to determine critical orbital parameters (Brown et al., 1978; Drissen et al., 1986). These parameters are essential for understanding the geometry and physical processes governing binary star systems. In the case of non-spherically symmetrical distribution of ejected material, orbital motion of the stars with respect to observer creates distinct polarization pattern that varies systematically with orbital phase. These patterns provide a direct probe of system's orbital parameters, such as inclination, the orientation of the orbit on the plane of the sky, and the direction of rotation, as well as the mass-loss rates and the structure of the circumstellar material (St. -Louis et al., 1988; Manset and Bastien, 2000; Abdul Qadir et al., 2023b, 2025).

In recent years, the study of polarized light has expanded to include exoplane-tary systems, a growing area of interest in modern astrophysics (Seager et al., 2000). Exoplanets are the planets that orbit stars outside our solar system and offer unique challenges and opportunities for polarimetric analysis. When starlight interacts with an exoplanet's atmosphere or surface, scattering processes polarize the light (Seager et al., 2000; Stam and Hovenier, 2005; Wiktorowicz, 2009). As the planet orbits its host star, the degree of polarization varies, making these signals an important probe of planetary characteristics (Seager et al., 2000; Lucas et al., 2009). This polarization, similar to that observed in binary star systems, can reveal critical information about the exoplanet's orbital parameters, including its inclination, orientation, and

rotation.

In a breakthrough study, Berdyugina et al. (2008) reported the first detection of polarized light from an exoplanet, HD 189733b. However, this finding was contested by Wiktorowicz (2009), who reported a non-detection of polarization from the same system. In response, Berdyugina et al. (2011) reaffirmed their detection of polarization originating from HD189733b. The first theoretical models of exoplanetary polarimetry, developed by Seager et al. (2000) and Fluri and Berdyugina (2010), demonstrated that polarization measurements could be used to probe atmospheric properties and surface albedo of close-in giant planets. This theoretical groundwork not only guided subsequent observational efforts, but was later employed by Wiktorowicz et al. (2015) to estimate the planetary albedo of HD 189733b. By analyzing the polarization signatures of exoplanets, astronomers can construct a detailed understanding of their atmospheres, orbital geometries, and evolutionary states, making polarimetry a uniquely powerful tool in exoplanetary studies.

However, detecting polarimetric signals from exoplanets using ground-based instruments has proven to be highly challenging, because of the small size of a planet compared to its host star or a secondary star in a binary system (Hough et al., 2006). The degree of polarization produced by an exoplanet is extremely weak, typically on the order of a few parts per million (PPM) (Seager et al., 2000; Berdyugina et al., 2008), which presents a significant challenge. As a result, only a small number of exoplanets, primarily the so-called "hot Jupiters" with high temperatures due to very close orbits have been targeted for polarimetric studies (Bott et al., 2016). Their proximity to their host stars and their thick scattering atmospheres make them potentially suitable for polarization observations with ground-based telescopes. Even when these weak signals are detected, modeling them remains a major challenge (Bailey et al., 2018). To date, there has been no comprehensive study that derived precise orbital parameters of an exoplanet using ground-based polarimetric observations.

To observe polarization with high precision, instruments such as DiPol-2 (Double Image Polarimeter - 2) and DiPol-UF (Double Image Polarimeter - Ultra Fast) must be employed, which are capable of measuring very weak polarization signals with high accuracy (Piirola et al., 2014, 2021). The data collected by such instruments undergo rigorous processes of data calibration and reduction (Piirola et al., 2014). Data treatment process also includes careful determination of instrumental (telescope) polarization and interstellar polarization (Kosenkov et al., 2017). Advanced algorithms are then applied to reveal intrinsic polarization signal. After these corrections, the final data are analyzed to derive key astrophysical parameters and physical properties of the observed system.

The investigation which was carried out in this thesis applies broadband high-precision optical polarimetry to studying physical properties and deriving orbital parameters for three O+O close binary star systems, AO Cas (Abdul Qadir et al.,

2023a), DH Cephei (DH Cep) (Abdul Qadir et al., 2023b), and HD 165052 (Abdul Qadir et al., 2025), and the exoplanet Upsilon Andromedae b ( $\upsilon$  And b). Each of these systems presents unique challenges and opportunities for study because of their distinct compositions, orbital characteristics, and circumstellar environments. The key objectives of this research include:

- 1. **Deriving Orbital Parameters**: This research aims to derive the orbital inclination, orientation, and rotational direction for each of the binary systems, utilizing polarization variability across their orbits. These parameters are crucial for constraining models of binary star interactions and understanding the geometry of the systems.
- Estimating Interstellar Polarization: Accurate estimation of interstellar polarization (ISP) is essential for separating intrinsic polarization effects from interstellar contributions. Observations of nearby field stars are incorporated to improve the estimation of ISP, ensuring more accurate polarization measurements for each binary system.
- 3. **Exploring Physical Properties**: This work investigates the scattering environments around each binary system by analyzing the phase-locked polarization variability. The study aims to provide new insights into stellar wind collisions and mass-loss processes. For the exoplanet v And b, we attempt to estimate the planetary geometrical albedo.

This thesis is organized as follows:

- Chapter 1 provides an introduction to astronomical polarimetry, including its applications to binary star systems and exoplanets.
- Chapter 2 discusses the theoretical background of polarization and mechanisms responsible for causing polarization in binary stars and exoplanets.
- Chapter 3 outlines the observational methods, data analysis techniques, and models used to interpret the polarization data.
- Chapter 4 presents the polarimetric data analysis of binary star systems and a summary of published papers included in this thesis.
- Chapter 5 presents the polarimetric data analysis of exoplanet v And b.
- Chapter 6 summarizes the key findings and implications of this research work.

# 2 Theoretical Background of Polarization, Polarimetry of Binary Stars, and Stars Hosting Exoplanets

Light, as an electromagnetic wave, consists of oscillating electric and magnetic fields, a concept first formalized by Maxwell (1865) in his theory of electromagnetism. The electric field component, specifically, is oriented in a direction perpendicular to the direction of propagation. Polarization refers to the specific orientation of the electric field vector of light waves, a phenomenon systematically described in optical physics since the early 19th century (Young, 1804; Fresnel, 1821). In unpolarized light, the electric field oscillates in random directions, with no preferential orientation. In contrast, polarized light exhibits a defined orientation of the electric field vector, making it sensitive to external influences such as scattering, reflection, and magnetic fields (Young, 1984). Understanding polarization is vital for analyzing astrophysical systems because it provides unique information about the geometric, physical, and dynamical properties of astronomical sources, as well as the processes occurring within them (Tinbergen, 2005). As mentioned earlier, astronomical polarization is always partial: only a fraction of light is polarized, with the remainder remaining unpolarized. This partial polarization carries signatures of the intervening medium and/or the intrinsic environment of the source. Polarimetric observations from binary stars and exoplanetary systems can potentially reveal details of the orbital geometry and physical properties of circumstellar and planetary environments.

## 2.1 Polarization of Electromagnetic Waves

The foundation of electromagnetic wave theory lies in Maxwell's equations, which describe how electric and magnetic fields propagate through empty space. These were first formulated in full by Maxwell (1865), building on work by Faraday and others, and are a cornerstone of classical electrodynamics (Heaviside, 1885; Rybicki and Lightman, 1979; Jackson and Fox, 1999):

$$\nabla \cdot \mathbf{E} = 0, \tag{1}$$

$$\nabla \cdot \mathbf{B} = 0, \tag{2}$$

$$\nabla \times \mathbf{E} = -\frac{\partial \mathbf{B}}{\partial t},\tag{3}$$

$$\nabla \times \mathbf{B} = \mu_0 \epsilon_0 \frac{\partial \mathbf{E}}{\partial t},\tag{4}$$

Here, **E** and **B** are electric and magnetic field vectors,  $\mu_0$  is the magnetic permeability, and  $\epsilon_0$  is the electric permittivity of free space. These equations describe how a time-varying electric field generates a magnetic field and vice versa, leading to the propagation of electromagnetic waves (Stratton and Chu, 1941; Rybicki and Lightman, 1979; Jackson and Fox, 1999).

For a plane electromagnetic wave traveling in the z-direction, the electric and magnetic fields can be expressed as:

$$\mathbf{E}(z,t) = E_0 \hat{x} \cos(kz - \omega t + \phi),\tag{5}$$

$$\mathbf{B}(z,t) = B_0 \hat{y} \cos(kz - \omega t + \phi),\tag{6}$$

where  $E_0$  and  $B_0$  are the amplitudes of the electric and magnetic fields, k is the wave number,  $\omega$  is the angular frequency, and  $\phi$  is the phase (Born and Wolf, 1959; Rybicki and Lightman, 1979; Jackson and Fox, 1999).

#### 2.2 Stokes Parameters

The state of polarization is quantitatively described by the four Stokes parameters, introduced by Stokes (1851), and further developed in the context of modern physics and optics (Chandrasekhar, 1960; Shurcliff, 1962). These parameters are essential for characterizing the polarization properties of light in a comprehensive and systematic manner (Shurcliff, 1962; Kliger et al., 1990; Hecht, 2017; Tinbergen, 2005). Understanding these parameters, that are also depicted by a schematic drawing in Figure 1, is critical for astronomers for measuring and interpreting polarization data.

The description of polarized light is most conveniently expressed using the Stokes formalism, in which the polarization state of a beam is represented by the Stokes vector:

$$S = \begin{bmatrix} I \\ Q \\ U \\ V \end{bmatrix}, \tag{7}$$

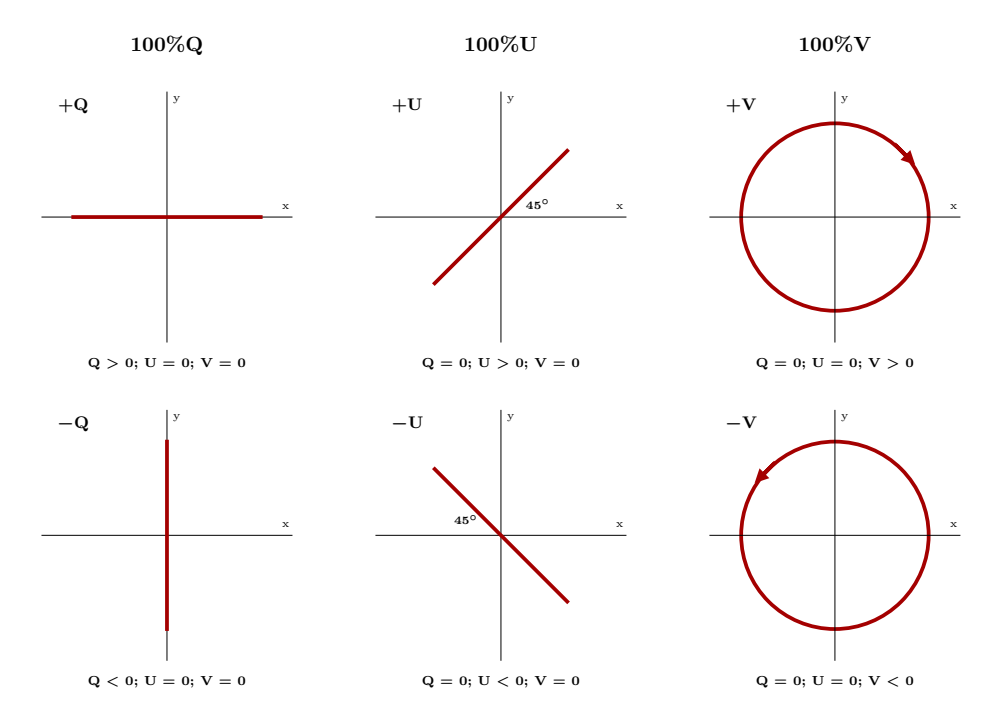


**Figure 1.** Schematic drawing of the three Stokes parameters. Q describes the linearly polarized intensity in the horizontal or vertical direction. U describes the same, but rotated over an angle of  $45^{\circ}$ . V describes the circularly polarized intensity.

where I is the total intensity, Q and U describe the linear polarization, and V represents the circular polarization. For the light wave described above, the four Stokes parameters are defined as:

• Stokes *I*: Total intensity of the light

$$I = E_x^2 + E_y^2, (8)$$

where  $E_x$  and  $E_y$  are the electric field amplitudes in the horizontal and vertical directions, respectively. This represents the total energy carried by the light across all polarization states, regardless of the orientation of the electric field. It gives a measure of the overall brightness of the source. A high value of I means a bright source, while a low value corresponds to a faint source.

 Stokes Q: Difference in intensity between horizontally and vertically polarized components

$$Q = E_x^2 - E_y^2. (9)$$

This parameter captures the linear polarization along two orthogonal axes (typically denoted as  $0^{\circ}$  and  $90^{\circ}$ ), providing a measure of the linear polarization along these directions.

Stokes U: Difference in the intensity between polarization components at 45° and 135°

$$U = 2E_x E_y \cos \delta, \tag{10}$$

where  $\delta$  is the phase difference between the horizontal and vertical components of the electric field. This parameter helps quantify the diagonal linear polarization, which is another important component of the total linear polarization, complementary to Stokes Q.

• Stokes V: Circular polarization component

$$V = 2E_x E_y \sin \delta. \tag{11}$$

It describes the degree of rotation of the electric field vector as the light propagates, distinguishing between right-handed and left-handed circular polarization.

The degree of total polarization (P) is given by:

$$P = \sqrt{Q^2 + U^2 + V^2}. (12)$$

Moreover, the polarization state is often characterized using normalized Stokes parameters, which are dimensionless quantities that express the fraction of each polarization component relative to the total intensity I:

$$q = Q/I, (13)$$

$$u = U/I, (14)$$

$$v = V/I. (15)$$

The degree of linear polarization ( $P_{lin}$ ) that is often referred as polarization degree (PD) in this work, is defined as:

$$P_{\rm lin} = \frac{\sqrt{Q^2 + U^2}}{I} = \sqrt{q^2 + u^2},\tag{16}$$

and polarization angle (PA) denoted by  $\theta$  is defined as:

$$\theta = \frac{1}{2}\arctan\left(\frac{U}{Q}\right). \tag{17}$$

The degree of circular polarization ( $P_{circ}$ ) is given by:

$$P_{\rm circ} = \frac{V}{I} = v. ag{18}$$

### 2.3 Polarization in Binary Star Systems

Polarization in binary star systems arises from various physical processes, each offering valuable diagnostic information about the system's geometry and the physical properties of its components. One significant mechanism responsible for polarization in these systems is scattering, which can occur due to free electrons, dust, or other particles in the circumstellar environment. Thomson scattering, involving the interaction of light with free electrons, is particularly important in systems with hot, massive stars, where intense radiation scatters off electrons, producing measurable polarization (Chandrasekhar, 1946; Brown and McLean, 1977; Brown et al., 1978). These studies have shown that polarization arising in such systems can be explained in terms of single Thomson scattering in optically thin circumstellar material. In systems containing Wolf-Rayet (WR) stars, spectropolarimetric observations have been utilized to investigate the structure and evolution of these massive binaries (Harries et al., 1998). These studies have shown that polarization arising in such systems can be explained in terms of single Thomson scattering in optically thin circumstellar material. In systems containing Wolf-Rayet (WR) stars, spectropolarimetric observations have been utilized to investigate the structure and evolution of these massive binaries (Harries et al., 1998). These observations clearly revealed the presence of hot ionized circumstellar gas emphasizing the role of scattering processes in shaping the polarization signatures observed in many WR binary systems. Moreover, the magnetic fields present in binary star systems can induce circular polarization through the Zeeman effect (Landi Degl'Innocenti and Landolfi, 2004). However, the study of circular polarization is beyond the scope of our work.

Early-type binaries, such as O+O binary systems composed of two massive O-type stars in close gravitational interaction, are particularly compelling for studying polarization due to their intense radiation fields and dynamic interactions. These systems are characterized by phenomena such as tidal distortions, mass transfer, and mass-loss via stellar winds, which create non-spherically symmetric distributions of circumstellar material (Rudy and Kemp, 1976; Berdyugin et al., 2016; Abdul Qadir et al., 2023a,b, 2025). Star light scattered on material ejected through stellar winds or mass transfer becomes linearly polarized, producing measurable polarization signals that vary with orbital phase. This makes O+O binaries ideal laboratories for probing orbital parameters, mass-loss rates, and the geometry of their circumstellar environments (Harrington and Collins, 1968).

The study of polarization variability across the binary's orbit provides critical parameters, such as the orbital inclination, the orientation of the orbit on the plane of the sky, and the direction of rotation (Brown et al., 1978; Drissen et al., 1986). These parameters are essential for understanding the geometry and physical processes that govern binary star systems. Additionally, the observed polarization can reveal the location of gaseous structures and probe their geometries, yielding additional infor-

mation on mass-loss processes and the interaction between stars (St. -Louis et al., 1988; Abdul Qadir et al., 2023b, 2025). This makes polarimetry a powerful tool for probing the physical conditions and evolutionary pathways of binary star systems.

## 2.4 Thomson Scattering in Binary Star Systems

In massive binary systems, stellar winds from each star can interact, creating a wind—wind collision region where free electrons scatter light from the stars. While a spherically symmetric wind produces no net polarization due to vector cancellation, the broken symmetry in the collision region generates a measurable polarization signal that varies with orbital phase. Thomson scattering (Thomson, 1906) occurs when electromagnetic radiation interacts with free electrons, producing linear polarization. This mechanism is particularly important in binary star systems with hot, massive stars, where electron densities are high. When unpolarized light from either stellar component is scattered by free electrons in the circumstellar environment, the scattered light becomes polarized. The degree and orientation of polarization depend on both the scattering angle and the spatial distribution of the electrons.

For a single scattering event, the transformation of the Stokes vector is described by the Müller matrix formalism. The Stokes parameters of the scattered light, S', are related to the incident Stokes vector S as (Chandrasekhar, 1960):

$$S' = \frac{f_{\text{Th}}}{2} \begin{bmatrix} 1 + \cos^2 \theta & \cos^2 \theta - 1 & 0 & 0\\ \cos^2 \theta - 1 & 1 + \cos^2 \theta & 0 & 0\\ 0 & 0 & 2\cos \theta & 0\\ 0 & 0 & 0 & 2\cos \theta \end{bmatrix} S, \tag{19}$$

where  $f_{\text{Th}}$  is the dilution factor,  $\theta$  is the scattering angle, and the transformation matrix represents the Müller matrix for Thomson scattering (Goldstein, 2003). This  $4 \times 4$  real matrix operates on the Stokes vector, providing a compact algebraic framework that describes how scattering processes generate and modify polarization.

For unpolarized incident light, the scattered radiation becomes polarized perpendicular to the scattering plane. The degree of polarization  $P(\theta)$  is given by:

$$P(\theta) = \frac{I_{\perp}(\theta) - I_{\parallel}(\theta)}{I_{\perp}(\theta) + I_{\parallel}(\theta)}.$$
 (20)

In this expression,  $I_{\perp}(\theta)$  and  $I_{\parallel}(\theta)$  represent the intensity components perpendicular and parallel to the scattering plane, respectively. For Thomson scattering of unpolarized incident light with intensity I, these components are defined as:

$$I_{\perp}(\theta) = \frac{f_{\rm Th}I}{2},\tag{21}$$

$$I_{\parallel}(\theta) = \frac{f_{\text{Th}}I}{2}\cos^2\theta. \tag{22}$$

In binary star systems, orbital motion causes time-dependent polarization variations as a result of changing scattering geometry with respect to the observer. Maximum polarization occurs when the system is viewed edge-on ( $\theta=90^{\circ}$ ), while constant polarization is observed when the system is viewed face-on ( $\theta=0^{\circ}$  or  $180^{\circ}$ ), and only the polarization position angle changes with orbital rotation. These variations provide insights into the system's inclination, orientation, direction of circumvention and distribution of the scattering electrons (Brown et al., 1978).

#### 2.5 Star Cluster Polarization

The observed polarization of star in open clusters arises from two main sources: intrinsic polarization from individual stars and interstellar polarization caused by dust grains within the cluster. The third polarization component may arise due to interstellar dust on the light of sight from observer to cluster. The wavelength dependence of polarization  $P(\lambda)$  caused by aligned interstellar dust grains can be described by empirical Serkowski's law (Serkowski et al., 1975):

$$P(\lambda) = P_{\text{max}} \exp\left(-K \ln^2 \frac{\lambda_{\text{max}}}{\lambda}\right), \tag{23}$$

where  $P_{\text{max}}$  is the maximum PD,  $\lambda_{\text{max}}$  is the wavelength at which the polarization reaches its maximum and K is an empirical parameter. Some studies, such as those by Wilking et al. (1980) and Whittet et al. (1992) have found an approximate linear relationship between K and  $\lambda_{\text{max}}$  in certain environments; however, this relationship is not universal.

The observed polarization of stars in the open clusters offers critical insights into the distribution of dust and geometry of magnetic field within the cluster providing information on the cluster evolutionary stage. By carefully disentangling these two components of polarization (or by intentionally choosing the cluster members with negligible intrinsic polarization), the properties of cluster dust can be derived and the interactions between stars and their surrounding environments can be investigated. The component of the interstellar polarization arising from the dust on the light path from the observer to the given cluster is assumed to be constant and has the same value and direction for all cluster stars. This approach not only enhances our understanding of the cluster's structure, but also provides valuable insights into its evolutionary processes (e.g., McMillan, 1976; Breger, 1982; Minniti et al., 1992;

Medhi et al., 2008; Eswaraiah et al., 2011; Singh and Pandey, 2020; Abdul Qadir et al., 2023b, 2025).

When stars within a cluster exhibit similar degrees of polarization and consistent position angles, it suggests that the cluster is evolved and has a uniform distribution of dust along the line of sight (e.g., McMillan, 1976; Feinstein et al., 2008; Abdul Qadir et al., 2023b). This uniformity indicates that the interstellar medium within the cluster has been homogenized over time, likely due to dynamical processes associated with the cluster's evolution. McMillan (1976) observed that the stars in the cluster NGC 7380 exhibited similar PDs and PAs, a finding later confirmed by Abdul Qadir et al. (2023b). This indicates that dynamical interactions between stars and the surrounding medium had likely caused the polarization to reach a more homogeneous state. Likewise, Feinstein et al. (2008) showed uniform galactic-aligned polarization in open cluster NGC 6250.

On the other hand, significant variations in PD or PA among the stars point to a non-uniform distribution of dust and variations in the orientation of the magnetic field. Such non-uniformity can arise from spatially varying dust densities, clumps in the inter-cluster medium, or multiple dust layers with distinct magnetic field geometries along the line of sight. Breger (1986) showed that light from the northwestern part of the Pleiades cluster passes through both foreground interstellar material and a patchy inter-cluster cloud. The presence of two superimposed clouds with differing magnetic field orientations led to partial cancellation (depolarization) of the net observed polarization, resulting in reduced PD values in that region of the cluster. Similarly, Eswaraiah et al. (2011) performed broadband polarimetric observations of the Galactic young open cluster Berkeley 59 and reported that the observed starlight appears to be depolarized due to non-uniform grain alignment in both foreground dust layers and the intracluster medium. Their study highlighted that polarization efficiency and alignment conditions can vary significantly even within a compact region, affecting the net polarization signature of each star. In a more recent study, Abdul Qadir et al. (2025) investigated the young open cluster NGC 6530 and found that nearly every observed member exhibited variations in both PD and PA, further supporting the presence of a complex, non-uniform dust and magnetic field environment within and surrounding the cluster. These findings reinforce the view that polarization studies offer a powerful diagnostic of dust and magnetic field structure, even on small spatial scales within stellar clusters.

Because many O+O binary systems are found as open cluster members, studying their intrinsic polarization necessarily involves measuring polarization of the nearby cluster stars for determination of the interstellar (or inter-cluster) polarization component. Thus, these measurements, made in the several passbands may serve two purposes: determination of intrinsic polarization component for the binary itself and studying cluster environment.

### 2.6 Polarization by Exoplanets

In addition to "traditional" binary star systems, the study of exoplanets through polarimetry is becoming an area of interest in modern astrophysics, as recent studies have begun to explore its potential for characterizing planetary atmospheres and surfaces (Seager et al., 2000; Berdyugina et al., 2011). Exoplanets are the planets that orbit stars outside our solar system and present unique challenges and opportunities for observation. The polarization of starlight reflected from an exoplanet's atmosphere provides valuable insight into its atmospheric properties, orbital geometry, and surface characteristics. When starlight interacts with the atmosphere or clouds of a planet, it becomes partially polarized, with the degree of polarization varying as the planet orbits its host star. However, detecting and modeling these polarization signals is extremely challenging due to their inherently weak nature, often on the order of a few PPM (Seager et al., 2000; Fluri and Berdyugina, 2010).

Hot Jupiters are prime targets for polarimetric studies due to their short orbital periods, high temperatures, and thick, scattering atmospheres (Seager et al., 2000). Their strong scattering properties make them more suitable for polarization measurements than smaller or cooler exoplanets. Polarimetric observations of hot Jupiters reveal amplitudes sensitive to high-altitude clouds, aerosols, and the distribution of scattering particles. However, because of their small size relative to their host stars, even these exoplanets exhibit polarization in the range of a few PPM to few tens of PPM at best. This makes detection challenging even with highly precise advanced instruments. Only a limited number of hot Jupiters can be observed polarimetrically using ground-based observations.

Phase-dependent polarimetry of exoplanets, particularly hot Jupiters, provides a potential means of determining geometric albedo and inferring aspects of atmospheric composition. Theoretically, the polarization signal is expected to vary with the planet's orbital position, reaching a maximum near quadrature phases when the planet is at its highest angular separation from the star (Seager et al., 2000; Stam and Hovenier, 2005). While direct observational detections remain very challenging due to the extremely weak signal, these variations, if measured, could reveal atmospheric structures such as reflective clouds or hazes and constrain the planet's orbital inclination and orientation. A major challenge is distinguishing reflected starlight from direct thermal emission, which requires both high-precision measurements and advanced modeling. Additional complications arise from noise introduced by Earth's atmosphere and potential contributions from stellar activity, such as spots on the parent star, which can affect the measured polarization (Carciofi and Magalhães, 2005; Lucas et al., 2009; Kostogryz et al., 2015). Future advancements in instrumentation, including space-based polarimeters, large ground-based telescopes, and techniques to account for stellar activity, may enable the detection and modeling of polarization signals from a wider range of exoplanets, including smaller and cooler exoplanets.

### 2.7 Rayleigh Scattering in Star-Exoplanet Systems

Just like planets in our solar system, Rayleigh scattering (Strutt, 1871) in the atmospheres of exoplanets is also the primary mechanism that can possibly produce a detectable polarization signal. Rayleigh scattering occurs when light interacts with particles much smaller than the wavelength of incident light (Bohren and Albrecht, 1998):

$$2\pi \frac{a}{\lambda}|m(\lambda)| \ll 1,\tag{24}$$

where a is the particle size,  $\lambda$  is the wavelength,  $m(\lambda) = n(\lambda) + ik(\lambda)$  is the complex refractive index, with the real part  $n(\lambda)$  corresponding to the phase speed of the wave in the medium, and the imaginary part  $k(\lambda)$  describing the extinction (van de Hulst, 1981).

While the PD caused by Rayleigh scattering depends on the scattering angle and the optical properties of the atmosphere, the intensity of Rayleigh scattering is highly sensitive to the wavelength of the incident radiation (Bohren and Albrecht, 1998):

$$S' = f_R \frac{1}{\lambda^4} \left| \frac{m(\lambda)^2 - 1}{m(\lambda)^2 + 2} \right|^2 M_{\text{Th}}(\theta) S, \tag{25}$$

where  $f_R$  is a proportionality factor,  $M_{\rm Th}(\theta)$  is the Mueller matrix, and S represents the incident light ray. If  $m(\lambda)$  varies slowly with  $\lambda$ , the intensity of the scattered radiation  $I_{\rm scat}$  is related to the incident intensity  $I_{\rm inc}$  by:

$$I_{\rm scat} \propto \frac{1}{\lambda^4} (1 + \cos^2 \theta) I_{\rm inc},$$
 (26)

where  $I_{\text{scat}}$  and  $I_{\text{inc}}$  are the intensities of scattered and incident radiation, respectively.

In a star system with an exoplanet, the polarization signal varies with the planet's orbital phase. Maximum polarization occurs near the quadrature phases ( $\theta=90^\circ$ ), while no polarization is observed during primary or secondary transits ( $\theta=0^\circ$  or  $180^\circ$ ). Additionally, the position angle of the polarization vector traces the projected orbit of the exoplanet, allowing for the determination of the orbital inclination and the planet's spatial orientation.

# 3 Polarimetric Instruments and Observations

The study of polarization in binary star systems and exoplanetary systems benefits significantly from advanced observational techniques, including optical broadband high-precision polarimetry. This method measures the degree and orientation of linear polarization across a wide range of optical wavelengths, providing critical insights into physical conditions, geometries, and scattering processes in these systems. Imaging polarimetry employs various techniques to measure the polarization state of light across extended sources, such as circumstellar disks and planetary atmospheres. This can be achieved using polarization filters, Wollaston prisms, or other optical elements that separate or modulate polarization states (Schmid et al., 2005, 2006; Quanz et al., 2011). Spectro-polarimetry, on the other hand, measures polarization as a function of wavelength across the spectrum, offering detailed information about the composition and dynamics of binary star atmospheres (Donati et al., 1997), and potentially the atmospheres of exoplanets.

Although optical broadband high-precision polarimetry is a powerful tool, complementary techniques from other wavelengths also contribute significantly to polarimetric studies. For instance, long-baseline interferometry in the radio, facilitated by observatories such as the Westerbork Synthesis Radio Telescope (WSRT; e.g., de Bruyn and Brentjens 2005), the Very Large Array (VLA; e.g., Perley et al. 2009), or MeerKAT (Jonas and the MeerKAT Team, 2016), provides polarimetric measurements tracing synchrotron or Faraday rotation processes, which probe physics other than light scattering. Polarimetry at ultraviolet, infrared, millimeter-wave, and high-energy wavelengths provides important complementary information to optical observations (e.g., Andersson et al. 2015; Planck Collaboration et al. 2020). Groundbased optical telescopes are essential for these studies, but they face challenges such as atmospheric distortions and wavelength absorption (Roddier, 1981). Space-based telescopes, such as the Hubble Space Telescope (HST) (Lupie and Stockman, 1988), bypass these limitations by observing polarization across ultraviolet, optical, and infrared wavelengths, offering clearer and more precise data. These instruments allow for the study of faint or distant objects without atmospheric interference. However, given the limited number of space-based telescopes capable of performing polarimetry, smaller ground-based telescopes are often employed when access to space-based instruments is not feasible.

#### 3.1 Polarimetric Instrumentation

Telescopes equipped with polarimeters or polarizing filters enable astronomers to analyze the light in various polarization states, often revealing subtle features not visible in regular imaging. Optical telescopes have traditionally been important instruments for ground-based polarimetric studies. By capturing light at different wavelength ranges, i.e. via broadband filters, they allow the study of polarization across various regions of the electromagnetic spectrum (Hough, 2006; Piirola et al., 2014).

In order to obtain accurate polarimetric data, the telescope's optical system must be carefully designed and calibrated to minimize instrumental polarization effects caused by the telescope itself, which can contaminate the measurements of the target's polarization (Keller, 2002). The precision of polarimetric measurements is largely dependent on the design of the telescope, its alignment, and the quality of its optical components. Telescopes with higher optical quality and stability provide more reliable results, especially when studying faint targets where the signal-to-noise ratio is low (Patat and Romaniello, 2006; Berdyugin et al., 2019).

For our polarimetric observations of binary star systems, we primarily used remotely operated 60 cm Tohoku T60 telescope (Haleakala Observatory, Hawaii, USA), and now retired, 60 cm KVA telescope (Observatory del Roque de los Muchachos, Canary Islands, Spain). The latest set of observations of exoplanet ups And b was obtained with 1 m C2PU telescope (Observatory Côte d'Azur, Plateau de Calern, France).

#### 3.1.1 T60 Telescope

Tohoku T60 telescope, located at the Haleakala Observatory in Hawaii, is a remotely operated 60 cm Cassegrain reflector and served as the primary telescope used for the observations in this study. It is equipped with a suite of instruments designed for high-precision photometric and polarimetric observations (Piirola et al., 2014). The telescope's remote operation capability, which includes a graphical user interface (GUI), allows for efficient and flexible scheduling of observations, making it an ideal facility for long-term monitoring campaigns of variable astrophysical sources such as binary star systems and exoplanets (Sakanoi et al., 2018). The T60 telescope is particularly well-suited for polarimetric studies due to its equatorial mount and precise tracking capabilities. Its optical design with Cassegrain focus minimizes instrumental polarization, ensuring high-quality measurements of astrophysical polarization signals (Sakanoi et al., 2018; Piirola et al., 2014).

#### 3.1.2 DiPol-2 Polarimeter

DiPol-2 operates on the principle of double-beam differential polarimetry, which allows it to measure polarization with high accuracy by simultaneously recording two orthogonal polarization states. Its design and operational principles are described in detail by Piirola et al. (2014). The instrument employs two dichroic beam-splitters to separate the incident light into three wavelength bands, enabling simultaneous multi-band observations in the B, V, and R passbands, or 400–800 nm. The dual-beam design of DiPol-2 is critical for minimizing systematic errors, as it cancels out common-mode noise (e.g., atmospheric fluctuations or telescope vibrations) that affects both beams equally. Additionally, DiPol-2 employs a rotating half-wave or quarter-wave plate to modulate the polarization state of the incoming light, enabling measurement of all four Stokes parameters (I, Q, U, and V). A schematic drawing of DiPol-2 is shown in Figure 2 and the key components of DiPol-2 are described below:

#### Modulator

Modulators are crucial in polarimetry as they systematically vary the polarization state of incoming light, allowing precise measurements (Serkowski et al., 1975; Tinbergen, 2005). DiPol-2 employs a rotatable superachromatic  $\lambda/2$  (or  $\lambda/4$ ) plate. The  $\lambda/2$  plate, or half-wave plate (HWP) being turned by angle  $\theta$  rotates the plane of linear polarization by  $2\theta$ , while the  $\lambda/4$  plate, or quarter-wave plate (QWP) converts linear polarization into circular polarization and vice versa. This modulation is used for determination of Stokes parameters. In order to further reduce systematic errors in measured linear polarization, DiPol-2 employs a beam-swapping technique with a complete rotation cycle of the half-wave plate. A half-wave plate rotates the plane of polarization by twice of the angle between the incident polarization direction and the plate's fast axis. Consequently, a mechanical rotation by 360° corresponds to a rotation of the polarization direction by 720°. In practice, beam swapping occurs every  $90^{\circ}$ , and a full measuring cycle in DiPol-2 consists of 16 exposures taken in  $22.5^{\circ}$ increments, ensuring cancellation of instrumental asymmetries due to dust particles, slight departures from plane parallelism, etc., and thereby improving the accuracy of the polarization measurements (Piirola et al., 2014).

#### Analyzer

Analyzers play a crucial role in a polarimeter by separating the orthogonal components of linearly polarized light. The simplest type is a polaroid that absorbs light polarized parallel to its optical axis (Tinbergen, 2005). Another type is the Glan–Thompson prism, which acts as a single-beam analyzer that measures only

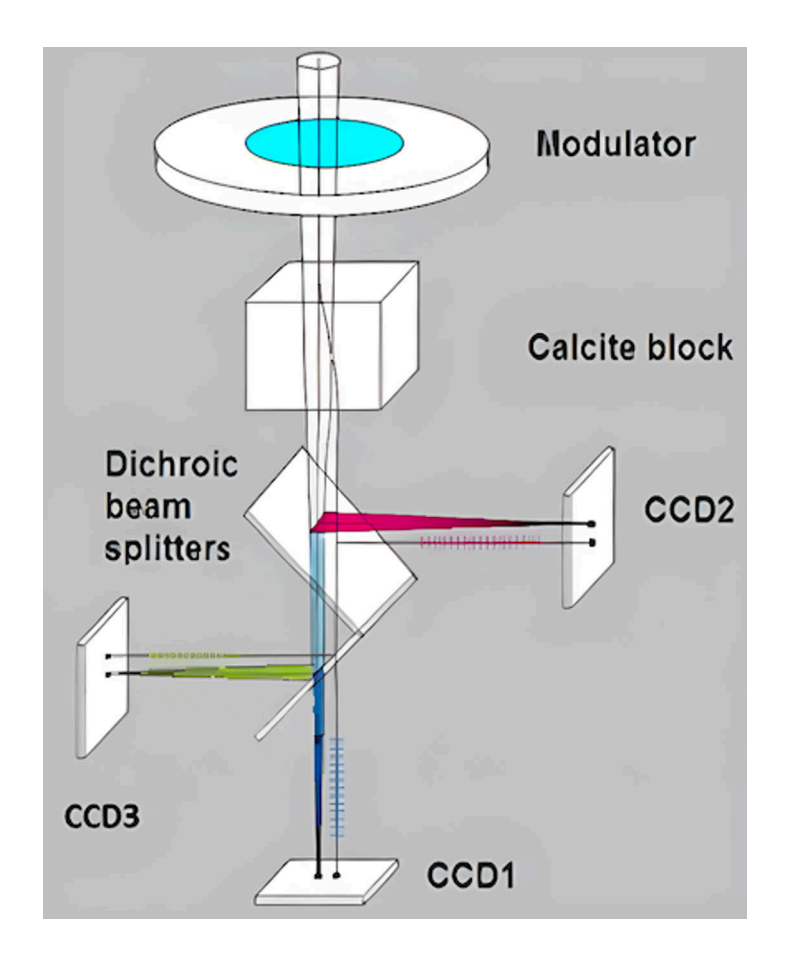


**Figure 2.** Layout of DiPol-2, showing components of the polarimeter. Image from Piirola et al. (2014).

one polarization component at a time. A major drawback of single-beam analyzers is that they lose half of the incoming light intensity (Tinbergen, 2005).

DiPol-2 uses a two-beam analyzer that exploits the birefringence property found in certain crystals. These crystals exhibit different refractive indices for light polarized along different axes, perpendicular to the principal direction (ordinary, or o-ray) and parallel to it (extraordinary, or e-ray). This difference causes the incoming light to split into two orthogonally polarized beams, each following a slightly different optical path (Serkowski et al., 1975; Tinbergen, 2005). Common two-beam analyzers include plane-parallel calcite plates, Savart plates, and Wollaston prisms (Serkowski et al., 1975; Tinbergen, 2005; Berdyugin et al., 2019). The ability to simultaneously measure both polarization components makes double-beam analyzers essential for achieving accurate and efficient polarimetric measurements. Dipol-2 employs a plane-parallel calcite plate as an analyser, which splits orthogonally polarized beams in parallel direction. In this way, the orthogonally polarized sky images are overlaid upon each of the doubled stellar images. Thus, contribution from sky polarization is optically eliminated.

#### Detectors

The DiPol-2 polarimeter employs three cooled CCD (Charge-Coupled Device) detectors, each dedicated to one of the spectral channels, B, V, and R. Wavelength separation is achieved with the use of two dichroic beam splitters placed after the Calcite block and directing each beam to its corresponding detector. This configuration enables simultaneous recording of orthogonally polarized stellar images across multiple passbands, enhancing both observational efficiency and precision (Berdyugin et al., 2019). This design allows making simultaneous multi-band observations, which are essential for studying wavelength-dependent polarization effects (Piirola et al., 2014).

The CCD detectors of DiPol-2 have low noise and high quantum efficiency, which are particularly important for detecting weak polarization signals from faint astronomical sources (Piirola et al., 2014). For bright stars, an intentional defocusing technique is employed to prevent saturation and collect of up to  $10^7$  photo-electrons per exposure (Berdyugin et al., 2019). Cooling the CCDs further reduces thermal noise, improving the signal-to-noise ratio and enabling the detection of subtle polarization variations (Berdyugin et al., 2019). This advanced detector system ensures that DiPol-2 can perform high-precision polarimetric measurements with minimal instrumental polarization, making it a reliable tool for diverse astronomical investigations (Piirola et al., 2014).

#### 3.2 Polarimetric Observations

A significant part of this work involved remote acquisition of polarimetric data of various targets over several years with DiPol-2 on T60 telescope. This setup allows for measurement accuracy down to approximately 0.001%, enabling the detection of even the most subtle polarization signals (Piirola et al., 2014). Such sensitivity is crucial for studying polarization effects arising from binary interactions, the scattering of light from circumstellar material, and the detection of polarimetric signatures from certain hot Jupiters.

Polarimetric observations with DiPol-2 require careful calibration, optimized exposure times, and precise data acquisition strategies to ensure high-precision results. As a part of the data calibration process, observations of unpolarized standard stars are regularly made to measure and correct for instrumental polarization, while polarized standard stars are observed to determine the instrument rotation, allowing transformation from instrumental to the standard equatorial sky reference system. In addition, bias, dark, and flat-field frames are regularly acquired to characterize detectors response and correct for systematic effects, thereby further improving accuracy of the final measurements.

Exposure times are selected on the basis of the brightness of the target and the desired signal-to-noise ratio (SNR). For bright stars, exposure times typically range from a few seconds to a minute, while fainter targets may require longer exposures, sometimes up to 3 minutes. Multiple exposures are taken for each target to enhance the SNR and mitigate the effects of atmospheric variability.

For linear polarization, a typical cycle of polarimetric measurement consists of 16 exposures at orientation intervals of 22.5° and for circular polarization, a cycle consists of 4 exposures at an orientation interval of 90° (Piirola et al., 2014; Berdyugin et al., 2019). In our case, for both binary stars and exoplanets observations by DiPol-2, we conducted linear polarization observations. For binary stars, we usually conducted 64–128 observations per night, and for exoplanets, we usually took 256–260 measurements per night. Intentional defocusing was implemented to prevent saturation while keeping the ordinary and extraordinary images well separated. The typical aperture size for defocused images was approximately 7–10 arcsec, with an o- and e-image separation of about 22 arcsec in the focal plane (Piirola et al., 2014). A real set of CCD images in the B, V, and R passbands are shown in Figure 3.

#### 3.3 Data Reduction

Raw images are pre-processed using standard techniques, including bias subtraction, dark frame subtraction, flat-fielding, and cosmic ray removal to correct for detector and optical system artifacts. These steps are automated using Visual Basic scripts that have been written and updated by several researchers in the department, in com-

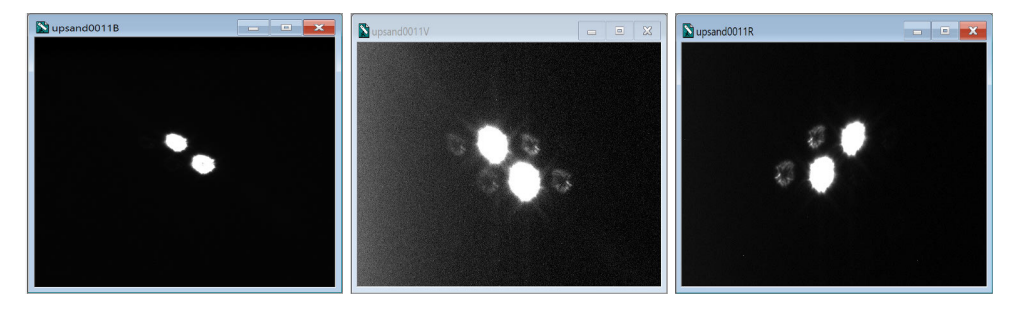


**Figure 3.** Defocused CCD images of images of v And in the B = 4400Å(left), V = 5500Å(center) and R = 7000Å(right) passbands. The faint "stars" visible on the V and R images are the reflections produced by dichroic beam splitters. They appear bright due to exaggerated contrast. In fact, the total intensity of reflection is < 0.1% of that produced by stellar image.

bination with MaxIM DL Pro software, <sup>1</sup> allowing efficient processing of hundreds of polarimetric images. After pre-processing, the intensities of the ordinary and extraordinary light components, produced by the polarizing optics as orthogonal projections of the incoming light, are measured and compared to derive the polarization signal (Piirola et al., 2014). This step is crucial for accurately measuring the polarization of the observed sources.

As mentioned earlier, a typical linear polarimetric observation involves several cycles of 16 exposures with the  $\lambda/2$  plate rotated in  $22.5^{\circ}$  increments. Each cycle provides four independent measurements of the linear polarization state. A prealignment algorithm is applied to correct image drift in long polarimetric sequences, and the data are binned  $2\times 2$  at the pixel level to reduce readout noise and enhance the signal-to-noise ratio (Piirola et al., 2014). Calibration is achieved through observations of zero-polarized and highly polarized standard stars, ensuring a typical final accuracy of approximately 0.001%-0.003% in the B passband and 0.002%-0.004% in the V and R passbands for the bright stars (Piirola et al., 2014).

Normalized Stokes parameters q and u are computed from the flux intensity ratios of the orthogonally polarized stellar images  $Q_{\rm i} = I_{\rm e}(i)/I_{\rm o}(i)$  obtained for each orientation of the wave plate,  $i=0.0^\circ, 22.5^\circ, 45.0^\circ, 67.5^\circ$ , as:

$$Q_{\rm m} = Q_{0.0} + Q_{22.5} + Q_{45.0} + Q_{67.5},$$

$$q = \frac{(Q_{0.0} - Q_{45.0})}{Q_{\rm m}},$$

$$u = \frac{(Q_{22.5} - Q_{67.5})}{Q_{\rm m}}.$$
(27)

The flux intensities  $I_{\rm e}(i)$  and  $I_{\rm o}(i)$  are extracted using aperture photometry, and

 $<sup>\</sup>overline{\mathbf{1}_{\text{https://diffractionlimited.com/downloads/GettingStarted.pdf}}$ 

the Stokes parameters are computed using a custom FORTRAN code. This code applies weighted averaging, assigning lower weights to measurements deviating from the mean of the set of measurements in that cycle by more than  $2\sigma$  and rejecting outliers beyond  $3\sigma$ . Final PDs and PAs are derived from the Stokes parameters. Systematic and statistical errors are carefully quantified to ensure the reliability of the polarization measurements. These errors include contributions from atmospheric conditions, instrumental effects, and photon noise.

In the follow-up polarization data analysis, methods such as Monte Carlo simulations or bootstrapping techniques are often employed to estimate uncertainties in the parameters derived from measured polarization. When performing polarimetric data analysis, one should take into account that an observed polarimetric signal from a star/exoplanet mainly contains the following types of polarization:

### 3.3.1 Intrinsic Polarization

Intrinsic polarization refers to the polarization of light that originates directly from the source or its immediate environment, reflecting the inherent properties of the system. In contrast, observed polarization is the total polarization measured by an observer, which can include contributions from additional sources such as interstellar dust, intervening material, or instrumental effects. While observed polarization is a composite signal, intrinsic polarization is specific to the source and provides direct insights into its geometry and physical processes. The proper data analysis of a polarimetric signal can only be performed by isolating the intrinsic polarization from the observed signal.

#### 3.3.2 Interstellar Polarization

Interstellar polarization (ISP) results from scattering and absorption of starlight by non-spherical dust grains aligned by the Galactic magnetic field in the interstellar medium. The efficiency of this alignment depends on grain properties, the local radiation field, gas density, and magnetic field strength. Early models assumed the Davis-Greenstein mechanism (Davis and Greenstein, 1951), while later studies included paramagnetic relaxation and other effects (Mathis, 1986; Li and Greenberg, 1997). More recent theoretical work emphasizes radiative torque (RAT) alignment, in which anisotropic radiation fields spin up irregular grains, aligning them with the magnetic field (Dolginov and Mitrofanov, 1976; Draine and Weingartner, 1996, 1997; Lazarian and Hoang, 2007).

ISP is typically uniform across relatively small fields of view and can be estimated for each target using nearby field stars located at similar distances. The observed degree of polarization depends on both the dust grain properties and the magnetic field orientation and usually follows a characteristic wavelength dependent.

dence described by Serkowski's empirical law (Section 2.5). Therefore, if a star expected to be intrinsically unpolarized exhibits non-negligible polarization with this wavelength dependence, the measured signal can be attributed primarily to interstellar polarization. Correcting for ISP is crucial to isolate the intrinsic polarization of astronomical sources, enabling accurate studies of their geometry and environments (Abdul Qadir et al., 2023a,b).

Interstellar extinction and polarization are closely related. The extinction law is described by the Cardelli, Clayton, and Mathis (CCM) model (Cardelli et al., 1989) and its extension by O'Donnell (1994):

$$\frac{A(\lambda)}{A_V} = a(\lambda) + \frac{b(\lambda)}{R_V},\tag{28}$$

where  $A(\lambda)$  is the extinction at wavelength  $\lambda$ ,  $A_V$  is the extinction in the V band,  $a(\lambda)$  and  $b(\lambda)$  are polynomials of  $1/\lambda$ , and  $R_V = \frac{A_V}{E(B-V)}$  is the ratio of total to selective extinction. The average value of  $R_V$  is approximately 3.1, but it can vary depending on the properties of the local ISM. The relationship between polarization and extinction can be expressed as:

$$\frac{P(\lambda)}{\tau(\lambda)} = \left\langle \frac{|C_{\parallel}(a,\lambda) - C_{\perp}(a,\lambda)|}{C_{\parallel}(a,\lambda) + C_{\perp}(a,\lambda)} \right\rangle_{\text{aligned}},\tag{29}$$

where  $\tau(\lambda)$  is the optical depth due to all grains, while  $C_{\parallel}$  and  $C_{\perp}$  represent the extinction cross-sections for radiation polarized parallel and perpendicular to the symmetry axis of the aligned grains, respectively. The average  $\langle \cdot \rangle_{\rm aligned}$  is taken over only the aligned grain population.

Recent empirical studies indicate that the maximum polarization efficiency, defined as  $P/A_V$ , can be significantly higher than the previously cited value of 3% per magnitude (Serkowski et al., 1975). For instance, Panopoulou et al. (2019) observed polarization efficiencies up to 13% per magnitude in certain regions of the interstellar medium. This relation is only approximate because  $R_V$  depends on the full grain population, whereas polarization arises from the aligned subset, making the connection between P and  $R_V$  more complex.

### 3.3.3 Instrumental Polarization

Instrumental polarization (IP) is introduced by the telescope and instrument optics and must be accounted for to ensure accurate polarization measurements. For our instrument, this is achieved by observing nearby ( $d \le 50~\rm pc$ ) standard stars from the list published by Piirola et al. (2021). All stars from this list can be used to measure instrumental polarization, and normally we observe different stars at the different areas of the sky. By measuring polarization of these standards, instrumental effects can be quantified and corrected, ensuring that the observed polarization signals are solely

attributable to the target object and the interstellar medium. Proper correction for instrumental polarization is essential for deriving reliable insights into the system's orbital parameters, mass-loss rates, and circumstellar dynamics. In our case, instrumental polarization is determined from observations of 10–15 nearby non-polarized stars compiled by Piirola et al. (2021), with typical values in the range  $(2-5)\times10^{-5}$  and measured with an accuracy of at least  $5\sigma$ . For calibration of the polarization angle zero-point, highly-polarized standard stars such as HD 204827, HD 161056, and HD 25443 were regularly observed (Turnshek et al., 1990; Piirola et al., 2021).

## 4 Polarimetry of Binary Stars

Once the polarimetric data are acquired and reduced, the next step is to analyze them. As mentioned earlier, in binary systems, the phase-locked variability of the polarization signal arises from Thomson scattering, i.e. the scattering of unpolarized stellar light by free electrons in the circumstellar environment (Brown et al., 1978). This scattering produces a polarization signal that varies periodically with the orbital motion, reflecting the changing projection of the system's geometry on the plane of the sky. To model this phase-dependent polarization, so-called BME (Brown, McLean, and Emslie) method (Brown et al., 1978), employs a model fit of the observed variations of the Stokes parameters with up to second-order Fourier series with orbital phase as an argument. Thus, this analytical approach relies on the best fit to the observed variations in Stokes q and u parameters with zero, first, and second harmonics of the phase of the orbital period. If the distribution of light scattering material is symmetric with respect to the orbital plane, the dominant contribution to the best fit comes from the second harmonics (Brown et al., 1978). The Fourier coefficients derived from these fits provide key information about the system's geometry, including the orbital inclination i and the longitude of the ascending node  $\Omega$  (Brown et al., 1978; Drissen et al., 1986).

### 4.1 Period Search

To identify periodic signals in time-series polarimetric data of binary stars and exoplanetary systems, we employed the Lomb-Scargle (LS) periodogram (Lomb, 1976; Scargle, 1982), a powerful algorithm well-suited for unevenly sampled astronomical data. Our implementation made use of the astropy.timeseries package in PYTHON<sup>2</sup> (Price-Whelan et al., 2018) and the spectral package in R<sup>3</sup> (Seilmayer and Ratajczak, 2017), both of which provide efficient tools for computing and visualizing periodograms.

The algorithm fits sinusoids to the data using a least-squares approach, making it particularly effective when the observing cadence is irregular due to weather, scheduling, or seasonal gaps. In binary and planetary systems with low eccentricity,

 $<sup>2 \\ \</sup>texttt{https://docs.astropy.org/en/stable/timeseries/lombscargle.html}$ 

 $<sup>\</sup>mathbf{3}_{\texttt{https://cran.r-project.org/web/packages/spectral/spectral.pdf}$ 

polarization signals induced by scattering are typically strongest when the scattering angle is  $90^{\circ}$  or  $270^{\circ}$ , and weakest at  $0^{\circ}$  or  $180^{\circ}$  (Brown et al., 1978; Seager et al., 2000). Consequently, the polarization varies twice per orbit, and the dominant peak in the periodogram usually corresponds to half the orbital period.

This behavior was consistently observed in our datasets for AO Cas, DH Cep, HD 165052. Periodograms for Stokes q and u in multiple passbands showed prominent peaks at approximately half the known orbital period. In all cases, we also observed alias peaks, which are produced when the detected period is not less than half of the sampling frequency, i.e., the Nyquist frequency ( $f_{\rm ny}$ ). In such cases, a side effect can occur that produces two waves differing by  $1/f_{\rm ny}$ . For example, the (half) orbital period for AO Cas is ~1.76 days, corresponding to a frequency of 0.57 d<sup>-1</sup>, which exceeds half the sampling frequency of ~0.4 d<sup>-1</sup> (based on 39 nights of observations over about 100 days). Therefore, an alias peak can be expected at 1/(1-1/1.76) = 2.31 days, which is exactly where the periodograms show an alias (Shannon, 1949; VanderPlas, 2018).

To assess the significance of detected peaks, we calculated false alarm probabilities (FAPs). While the FAPs varied depending on data quality, they were always negligible ( $\ll 1\%$ ) for the binary star datasets. The LS method proved very effective for our datasets, it yielded a more precise determination of the orbital period for HD 165052 compared to the value recently derived by Rosu et al. (2023).

### 4.2 BME Method

The most common method to study the phase curves of the Stokes parameters q and u variation for a binary star system is the expansion of observed periodic variations with a Fourier series up to the second harmonics. This approach, often referred to as the BME method (Brown et al., 1978), can be applied to systems with circular or nearly circular orbits.

Let us consider the geometry of Thomson scattering from a single star, as shown in Figure 4. A Cartesian coordinate system (x,y,z) is established with its origin at the illuminating point source, star O, and the x-axis directed toward the observer on Earth. The z-axis lies in the plane of the sky. The analysis considers the scattering of unpolarized light from this source by a single electron at a location P, defined by spherical coordinates  $(r,\theta,\phi)$ . The light incident on the electron at P is scattered through an angle  $\chi$  into the line of sight. For Thomson scattering, this process produces linear polarization perpendicular to the local scattering plane, whose orientation is defined by the unit vector  $\mathbf{n}$ . The relations between the Cartesian coordinates at P and the scattering angles  $(\chi,\psi)$  are given by:

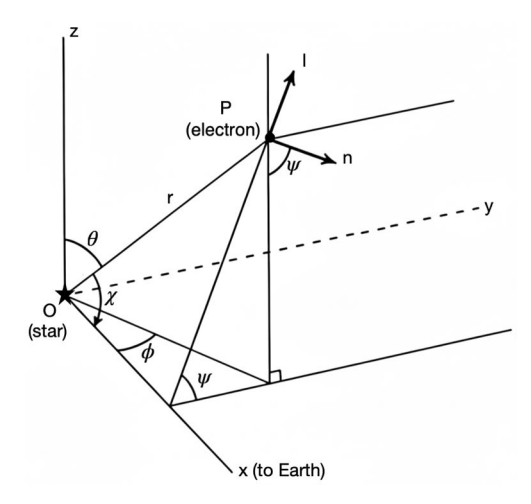


**Figure 4.** Scattering geometry for a single point source. The coordinate system is centered on the star O, with the x-axis pointing toward the observer. Light is scattered at point  $P(r, \theta, \phi)$  through an angle  $\chi$ . The unit vector  $\mathbf{n}$  lies in a plane perpendicular to the line of sight and defines the direction of polarization. Adapted from Brown et al. (1978).

$$x/r = \sin\theta\cos\phi = \cos\chi,\tag{30}$$

$$y/r = \sin\theta\sin\phi = \sin\chi\cos\psi,\tag{31}$$

$$z/r = \cos\theta = \sin\chi\sin\psi. \tag{32}$$

These expressions allow  $\chi$  and  $\psi$  to be eliminated from the scattering integrals so that the Stokes parameters for singly scattered light can be expressed directly in terms of the electron density distribution  $n(r,\theta,\phi)$ . The total observed Stokes parameters I,Q, and U are obtained by integrating over the entire envelope. The integrations for the Stokes parameters may be expressed as:

$$I_2 = I_0 \sigma_0 \int_0^\infty \int_0^\pi \int_0^{2\pi} n(r, \theta, \phi) (\sin^2 \theta \sin^2 \phi - \cos^2 \theta) \sin \theta \, dr \, d\theta \, d\phi, \quad (34)$$

$$I_3 = I_0 \sigma_0 \int_0^\infty \int_0^\pi \int_0^{2\pi} n(r, \theta, \phi) (\sin 2\theta \sin \phi) \sin \theta \, dr \, d\theta \, d\phi. \tag{35}$$

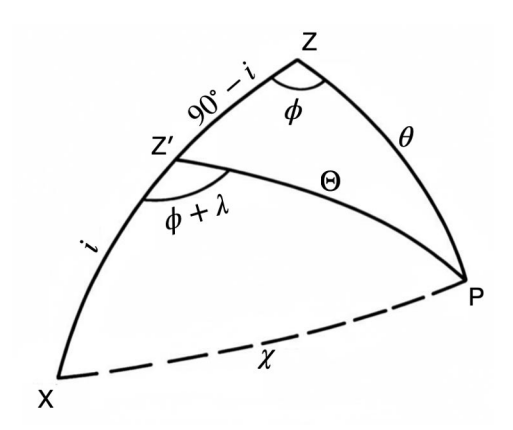


**Figure 5.** Spherical triangle used to transform from the line-of-sight coordinate system of Figure 4 to a coordinate frame corotating with the binary pair  $O_1, O_2$ . For either component star, the z'-axis is perpendicular to the orbital plane. The point  $P(R, \Theta, \Phi)$  represents a general position, while Ox, Oz, and Oz' lie in the same plane. The quantity  $\lambda$  denotes the longitude of the binary pair measured from the reference plane zz'x. Adapted from Brown et al. (1978).

The factor  $I_0$  denotes the incident (unscattered) intensity, serving as a normalization for the scattered components. The quantities  $I_1$ ,  $I_2$ , and  $I_3$  correspond to the integrated intensities along the coordinate axes associated with the Stokes parameters I, Q, and U, respectively, where  $Q = I_2/I$  and  $U = I_3/I$ . The coefficient  $\sigma_0$  represents the scattering cross-section per particle, describing the efficiency with which an individual scatterer redirects the incident radiation. The expressions in parentheses represent the angular dependence of the scattered radiation, characteristic of Thomson scattering, which can be generalized to multiple illuminating sources as:

$$I = \sum_{j=1}^{N} I_j, \quad Q = \sum_{j=1}^{N} f_j Q_j, \quad U = \sum_{j=1}^{N} f_j U_j,$$
 (36)

where  $I_j$  denotes the total scattered intensity from the  $j^{\rm th}$  source, and  $f_j = I_j / \sum_{j=1}^N I_j$  gives its fractional contribution to the system's total scattered flux.

Using the coordinate transformation illustrated in Figure 5, the expressions for the total intensity and the normalized Stokes parameters can be rewritten in terms of the orbital longitude  $\lambda$  and inclination i. By substituting these transformations into Equations (33) – (35), and noting that i and  $\lambda$  are independent of the integration coordinates, the equations can be systematically arranged according to the Fourier terms in  $\lambda$ , yielding:

$$I = I_0 [1 + \tau_0 \{ 2(1 + \gamma_0) + (1 - 3\gamma_0) \sin^2 i + G \sin 2i \cos(\lambda + \lambda_1) + H \sin^2 i \cos 2(\lambda + \lambda_2) \} ],$$
(37)

$$Q = \tau_0 \{ (1 - 3\gamma_0) \sin^2 i + G \sin 2i \cos(\lambda + \lambda_1) \}$$

$$-H(1+\cos^2 i)\cos 2(\lambda+\lambda_2)\},\tag{38}$$

$$U = 2\tau_0 \{ G \sin i \sin(\lambda + \lambda_1) - H \cos i \sin 2(\lambda + \lambda_2) \}, \tag{39}$$

where  $\tau_0$  is the mean optical depth of the scattering envelope. The parameters G and H describe the relative amplitudes of the first and second harmonics, respectively, defined as:

$$\tan \lambda_1 = \frac{\gamma_2}{\gamma_1}, \quad \tan 2\lambda_2 = \frac{\gamma_4}{\gamma_3}, \tag{40}$$

$$G = \sqrt{(\gamma_1^2 + \gamma_2^2)}, \quad H = \sqrt{(\gamma_3^2 + \gamma_4^2)}.$$
 (41)

Parameters  $\gamma_0, \gamma_1, \gamma_2, \gamma_3$ , and  $\gamma_4$  (given by equations (7) in Brown et al. (1978)) represent a set of optical depths integrated over solid angle, with various weighting over direction, and averaging between the two stars weighted according to their brightness. Parameter  $\gamma_0$  can be seen as an inverse measure of the effective degree of flattening of the envelope toward the orbital plane. Parameters  $\gamma_1, \gamma_2$  and their amplitude parameter G measure the effective degree of asymmetry of light scattering material with respect to orbital plane. These parameters contribute to the amplitudes of the first-harmonic terms in the Fourier representation.

At the same time,  $\gamma_3$ ,  $\gamma_4$  and H measure effective degree of concentration of material toward the orbital plane and provide contribution to the amplitudes of the second-harmonic terms. The quantities G and H represent the total amplitudes of the first and second harmonics, respectively, and  $\lambda_1$  and  $\lambda_2$  denote their respective phase angles. It is sometimes convenient to refer to the ratio of these harmonic amplitudes as a relative amplitude A = H/G, and to the difference  $\Delta\lambda = \lambda_1 - \lambda_2$  as a phase difference between the first and second harmonics. These relations provide the analytical foundation for interpreting the observed periodic variations in polarization using the BME method.

The formalism described above simplifies considerably for the important case of an envelope that is symmetric with respect to the orbital plane. In this configuration, the density distribution is mirror-symmetric above and below the plane, which forces the first-harmonic coefficients to zero ( $\gamma_1 = \gamma_2 = 0$ , and hence G = 0). Consequently, the variations in the Stokes parameters Q and U are governed solely by the second harmonic in the orbital longitude  $\lambda$ . The resulting locus traced in the (Q,U) plane over an orbital period is an ellipse, which is traversed twice per orbit.

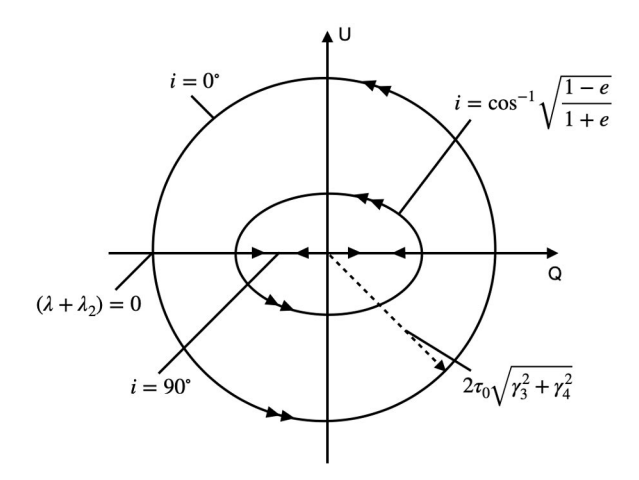


**Figure 6.** Relationship of the properties of all envelopes with material concentrated in or symmetric about the orbital plane to the eccentricity, size, and orientation of the resulting elliptical Q, U locus (executed twice per orbit). Adapted from Brown et al. (1978).

The geometry of this ellipse provides a direct diagnostic for the orbital inclination i. As illustrated in Figure 6, for a pole-on system  $(i=0^\circ)$  the locus is a circle, while for an edge-on system  $(i=90^\circ)$  it degenerates to a straight line. The eccentricity e of the ellipse is related to the orbital inclination by:  $i=\cos^{-1}\sqrt{\frac{1-e}{1+e}}$ . The direction of circumvention of the ellipse shown on Figure 6 corresponds to direction of rotation in binary system as seen on the plane of the sky. The semi-major axis of the ellipse has magnitude  $\tau_0 H(1+\cos^2 i)$  and the semi-minor axis has magnitude  $2\tau_0 H\cos i$ . The center of the ellipse C is offset from the origin by the constant polarization term  $\tau_0 (1-3\gamma_0)\sin^2 i$ . An additional offset can be introduced by constant ISP component.

The phase parameter  $(\lambda + \lambda_2) = 0$  indicated in Figure 6 defines the starting point of the locus on the polarization ellipse, corresponding to the orientation of the binary system at the reference orbital phase. This phase relationship determines where on the ellipse the polarization vector begins its path and provides information about the azimuthal distribution of scattering material relative to the binary components. When the ellipse is plotted in the standard equatorial coordinate system defined by the Stokes parameters (q, u), the axes represent the normalized linear polarization components along fixed directions on the plane of the sky: q measures the polarization aligned with or perpendicular to the celestial north–south axis, while u measures the polarization oriented at  $45^{\circ}$  to that axis. Hence, the orientation of the line  $(\lambda + \lambda_2) = 0$  (e.g., the ellipse's major axis) in the (q, u) plane corresponds to the projected orientation of the binary orbit on the sky. Building upon this analytical framework, the observed periodic variations in the Stokes parameters q and u are typically modeled using a Fourier series, directly connecting the theoretical formalism to measurable polarization variations as a function of orbital phase:

$$q = q_0 + q_1 \cos \lambda + q_2 \sin \lambda + q_3 \cos 2\lambda + q_4 \sin 2\lambda,$$
  

$$u = u_0 + u_1 \cos \lambda + u_2 \sin \lambda + u_3 \cos 2\lambda + u_4 \sin 2\lambda,$$
(42)

where  $\lambda = 2\pi\phi$  and  $\phi$  is the orbital phase. The coefficients  $q_i$  and  $u_i$  are determined through a fitting process, providing a detailed description of the polarization behavior as a function of orbital phase. These coefficients are crucial for extracting physical information about the system.

One of the key parameters that can be derived from the Fourier coefficients is the orbital inclination i. The inclination is a measure of the tilt of the orbital plane relative to the observer's line of sight and can be calculated using the first and second harmonic terms. The following relations are used to determine i (Brown et al., 1978; Drissen et al., 1986):

$$\left(\frac{1-\cos i}{1+\cos i}\right)^4 = \frac{(u_1+q_2)^2 + (u_2-q_1)^2}{(u_2+q_1)^2 + (u_1-q_2)^2},$$
or
$$\left(\frac{1-\cos i}{1+\cos i}\right)^4 = \frac{(u_3+q_4)^2 + (u_4-q_3)^2}{(u_4+q_3)^2 + (u_3-q_4)^2}.$$
(43)

In most binary systems, the light-scattering material is symmetrically distributed relative to the orbital plane. In such cases, the first harmonic terms are often negligible, so the polarization variability is dominated by the second harmonic (see Abdul Qadir et al. (2023a,b, 2025)). This simplifies the analysis and allows for a more straightforward determination of the orbital inclination. In addition to the inclination, orientation of the orbit (the longitude of the ascending node  $\Omega$ ) and direction of circumvention on the plane of the sky can also be determined. The  $\Omega$  can be calculated using the following equations (Brown et al., 1978; Drissen et al., 1986):

$$\tan \Omega = \frac{A+B}{C+D} = \frac{C-D}{A-B},\tag{44}$$

where the quantities A, B, C, and D are defined as:

$$A = \frac{u_4 - q_3}{(1 - \cos i)^2}, \quad B = \frac{u_4 + q_3}{(1 + \cos i)^2},$$

$$C = \frac{q_4 - u_3}{(1 + \cos i)^2}, \quad D = \frac{u_3 + q_4}{(1 - \cos i)^2}.$$
(45)

The orientation  $\Omega$  provides information about the alignment of the binary system relative to the observer and is essential for understanding the three-dimensional geometry of the system.

Another important aspect of the analysis is the ratio of the amplitudes of the second to first harmonics for the Stokes parameters q and u. These ratios, denoted as  $A_q$  and  $A_u$ , provide insights into the symmetry and concentration of the scattering material relative to the orbital plane. They are calculated as:

$$A_q = \sqrt{\frac{q_3^2 + q_4^2}{q_1^2 + q_2^2}}, \quad A_u = \sqrt{\frac{u_3^2 + u_4^2}{u_1^2 + u_2^2}}.$$
 (46)

For systems with a high degree of symmetry, the second harmonic terms dominate, resulting in large values of  $A_q$  and  $A_u$ . Conversely, deviations from symmetry can lead to significant first harmonic contributions, which may indicate asymmetries in the distribution of scattering material.

The derived values of i,  $\Omega$ ,  $A_q$ , and  $A_u$  are typically consistent across different passbands (Abdul Qadir et al., 2023a,b, 2025), demonstrating the robustness of the method. However, potential biases in the inclination i must be considered, as Fourier-derived inclinations tend to be overestimated, especially for systems with low true inclinations. Lower true inclinations tend to result in larger biases, and these can be corrected using statistical methods (Aspin et al., 1981; Simmons et al., 1982; Wolinski and Dolan, 1994). Non-periodic polarization variability further amplifies this bias (Manset and Bastien, 2000). For low inclinations ( $i < 45^{\circ}$ ), especially in low-eccentricity orbits, the BME method systematically overestimates i and produces asymmetric confidence intervals that extend to  $i = 0^{\circ}$ . In non-eclipsing systems, this limits polarimetric data to providing only an upper bound on i. Furthermore, as i decreases, confidence intervals for the position angle ( $\Omega$ ) also widen. To quantify this bias and the confidence intervals for i and  $\Omega$ , the "figure of merit" parameter  $\gamma$  defined by Wolinski and Dolan (1994) can be used.

$$\gamma = \left(\frac{A}{\sigma_{\rm p}}\right)^2 \frac{N}{2},\tag{47}$$

where A is the amplitude of polarization variability:

$$A = \frac{|q_{\text{max}} - q_{\text{min}}| + |u_{\text{max}} - u_{\text{min}}|}{4},$$
(48)

 $\sigma_{\rm p}$  is the standard deviation of the Stokes parameters around the best-fit curve, and N is the number of observations.

While analyzing polarimetric data of HD 165052, we conducted Monte Carlo simulations to derive  $1\sigma$  and  $2\sigma$  confidence intervals for i and  $\Omega$  (Abdul Qadir et al., 2025). Like previous studies (Wolinski and Dolan, 1994; Manset and Bastien, 2000), we used simulated data, but unlike previous studies, we used actual errors and phase sampling for more precise evaluation of confidence intervals. We modeled Stokes

parameters for i ranging from  $90^\circ$  to  $180^\circ$  using BME model and added Gaussian noise with variance  $\sigma^2=0.5NA^2/\gamma$ . The results of these simulations are discussed in Abdul Qadir et al. (2025).

### 4.3 Mass-Loss Rate

It is possible to estimate the mass-loss rate from the component(s) in an O-type binary star system using polarization variability amplitude, employing the method proposed by St. -Louis et al. (1988). The method utilizes the polarization variability amplitude  $A_{\rm p}$ , defined as

$$A_{\rm p} = \tau_0 H(1 + \cos^2 i),\tag{49}$$

where  $\tau_0 H$  is the optical depth moment. Here, a *moment* refers to a weighted measure of the optical depth, in which each part of the scattering material contributes according to its geometry and relative effect on the observed polarization. It is given by Drissen et al. (1986) as the following:

$$\tau_0 H = \sqrt{\frac{q_3^2 + q_4^2}{L^2 + M^2}} = \sqrt{\frac{u_3^2 + u_4^2}{N^2 + R^2}},\tag{50}$$

where:

$$L = (1 + \cos^2 i)\cos\Omega, \quad M = 2\cos i\sin\Omega,$$
  

$$N = (1 + \cos^2 i)\sin\Omega, \quad R = 2\cos i\cos\Omega.$$
(51)

As shown by St. -Louis et al. (1988), in the case of Wolf-Rayet (WR)+O system, the mass-loss rate due to stellar wind from the primary component can be estimated using the following formula:

$$\dot{M} = \frac{(16\pi)^2 m_{\rm p} v_{\infty} a A_{\rm p}}{(1 + \cos^2 i) 3\sigma_{\rm t} f_{\rm c} I},\tag{52}$$

where M is the mass-loss rate,  $f_{\rm c}$  is the fraction of total light from the companion star,  $v_{\infty}$  is the wind terminal velocity, a is the semi-major axis,  $m_{\rm p}$  is mass of proton,  $\sigma_{\rm t}$  is Thomson cross section, and I is a specific integral:

$$I = \int_0^\infty \int_0^\pi \int_0^{2\pi} \frac{\sin^3 \theta \cos 2\phi d(R/a) d\theta d\phi}{(R'/a)^2 (1 - R_*/R')^\beta}.$$
 (53)

Note that primed coordinates are measured relative to the primary star, while unprimed coordinates originate at the secondary star. In order to evaluate this integral, one has to choose a specific wind velocity law:  $v(R') = v_{\infty}(1 - R_*/R')^{\beta}$ , characterized by the parameter  $\beta$ .

In a WR+O binary system, the WR star's strong stellar wind is the primary source of polarization, while the O-type companion, despite contributing to the total light, has a much weaker wind and polarization is diluted by the unpolarized WR star light. To correct for this dilution when deriving the WR star's mass-loss rate  $(\dot{M})$ , the observed polarization amplitude  $(A_{\rm p})$  is divided by the O-star's fractional light contribution  $(f_{\rm c})$ . In an O+O binary system, both stars contribute comparably to the observed polarization, leading to roughly equal polarization and dilution effects. Thus, for typical O+O system, one can assume  $f_{\rm c}=0.5$  for each component. Additionally, we must account for the difference in wind composition (Abdul Qadir et al., 2025). The WR wind, composed of He, has an electron-to-nucleon ratio of  $\alpha_{\rm WR}=0.5$  for fully ionized helium, while the O-star wind, primarily composed of 90% H and 10% He, has a ratio of approximately 1.0. This leads to the following expression for the mass-loss rate of an O+O binary system (Abdul Qadir et al., 2025):

$$\dot{M} = \frac{(16\pi)^2 m_{\rm p} v_{\infty} a A_{\rm p}}{(1 + \cos^2 i) 3\sigma_{\rm t} f_{\rm c} I} \cdot \frac{1}{2},$$
or
$$\dot{M} [M_{\odot} \text{ yr}^{-1}] = \frac{1.16 \times 10^{-7} v_{\infty} (\text{km s}^{-1}) a (R_{\odot}) A_{\rm p}}{(1 + \cos^2 i) f_{\rm c} I}.$$
(54)

### 4.4 Summary of Publications

The data analysis techniques outlined in this chapter have been effectively applied to three binary star systems and described in three publications included in this thesis. The author served as the Principal Investigator (PI) for all three studies. Polarimetric observations were primarily carried out by the author in collaboration with the primary supervisor, Doc. Andrei Berdyugin. Data reduction was performed either by the author or by Doc. Berdyugin. The initial drafts of all manuscripts were written by the author, with subsequent thorough revisions and edits provided by Doc. Berdyugin. Final versions were shared with co-authors only after review and approval by both the PI and the primary supervisor, at which point additional feedback was incorporated. The summary of these papers is as follows:

# 4.4.1 Paper I – High-precision broadband linear polarimetry of early-type binaries III. AO Cassiopeiae revisited

AO Cassiopeiae (AO Cas) is a well-studied O-type binary system observed through optical polarimetry, exhibiting phase-locked polarization variability. Our analysis of polarimetric data clearly revealed an unambiguous periodic signal at 1.76 d, half of the known orbital period of the binary system. We detected phase-locked variations

in the Stokes parameters q and u across all three passbands: B, V, and R, using DiPol-2. Fourier fits showed strong second harmonics with small but non-zero first harmonics, particularly in the variability of the Stokes u parameter, at a significance level of approximately  $2\sigma$ . Notably, the presence of first harmonics is also apparent in the data obtained by Rudy and Kemp (1976), suggesting a slight asymmetry in the scattering material relative to the orbital plane of AO Cas. A comparison with historical data indicates that the polarization curve has remained stable over decades, although subtle asymmetries point to inhomogeneities in the scattering environment. Additionally, we successfully derived the interstellar polarization by observing three non-polarized stars in the vicinity of AO Cas. From a two-harmonic Fourier fit, we derived an orbital inclination of  $i=63^{\circ}+2^{\circ}/-3^{\circ}$  and an orientation of  $\Omega=29^{\circ}(209^{\circ})\pm 8^{\circ}$ , consistent with independent determinations.

# 4.4.2 Paper II – High-precision broadband linear polarimetry of early-type binaries IV. The DH Cephei binary system in the open cluster of NGC 7380

DH Cep is a massive O + O-type binary system for which our observations clearly revealed, for the first time, phase-locked polarization variability along the binary orbit with an amplitude of approximately 0.2%. Lomb-Scargle periodogram analysis confirmed a dominant signal at half the orbital period (2.11 d). In addition to the periodic variability, we detected significant non-periodic fluctuations, likely caused by wind inhomogeneities. The intrinsic polarization, estimated at 0.6% after accounting for interstellar contributions, indicates a non-spherical scattering envelope. Furthermore, observations of 14 field stars in the NGC 7380 cluster revealed uniform PDs and PAs, indicating a coherent alignment of dust grains along the line of sight. While this could reflect the dust distribution within the cluster itself, contributions from the foreground interstellar medium may also play a role. A Fourier fit to the data provided an orbital inclination of  $i=46^{\circ}+11^{\circ}/-46^{\circ}$  and an orientation of  $\Omega=105^{\circ}\pm55^{\circ}$ , consistent with previous determinations. The estimated mass-loss rate of  $3.4\times10^{-7}M_{\odot}{\rm yr}^{-1}$  aligns with values derived using other methods.

### 4.4.3 Paper III – High-precision broadband linear polarimetry of early-type binaries. V. The Binary System HD 165052 in Open Cluster NGC 6530

HD 165052 is a massive O+O-type binary system located in the young open cluster NGC 6530. Our high-precision broadband polarimetric studies revealed for the first time periodic polarization variability in the Stokes q and u parameters with an orbital period of  $2.95510 \pm 0.005$  d and amplitude of approximately 0.2%. Our independent period search, performed on the polarization data, supports a shorter

orbital period for HD 165052, contradicting the slightly longer value derived from radial velocity (RV) measurements in a recent study. Polarimetric observations of two dozen nearby stars in NGC 6530 revealed complex interstellar polarization behaviour, indicating a non-uniform dust distribution, as expected in such a young stellar cluster. The variations in the Stokes q and u parameters are dominated by the second harmonic, suggesting a symmetric distribution of scattering material, likely due to interacting stellar winds. From a two-harmonic Fourier fit, we derived the best estimate of the orbital inclination as  $i = 55^{\circ} + 5^{\circ} / - 55^{\circ}$  and the orientation as  $\Omega = 148^{\circ}(328^{\circ}) + 20^{\circ}/-22^{\circ}$ , averaged over the B, V, and R passbands. However, since HD 165052 is a non-eclipsing binary with a low inclination, the inclination value derived from polarimetry cannot be considered highly accurate. To verify this, we performed simulations which confirm that polarimetric analysis cannot reliably detect inclinations below approximately 45°, instead returning artificially higher values. The estimated mass-loss rate for the entire system is  $\dot{M} = 3.47 \times 10^{-7} \pm 1.59 \times 10^{-8} M_{\odot} \text{ yr}^{-1}$ , consistent with values obtained through other methods.

## 5 Polarimetry of Exoplanet v And b

Similar to binary star systems, polarimetry of exoplanets can help determine their orbital geometry and physical properties. The observed polarization signal may arise from Rayleigh scattering of starlight by atmospheric particles and molecules (Strutt, 1871), producing phase-dependent variations in the Stokes q and u parameters. These variations can be modeled to constrain orbital parameters such as inclination, orientation angles, and the planet's geometrical albedo. The Rayleigh–Lambert (RL) approximation models this variability by treating the planet as a Lambertian scatterer with Rayleigh-induced polarization (Seager et al., 2000; Wiktorowicz, 2009).

The faint signal from an exoplanet is easily diluted by the star's glare, making direct observations extremely challenging. Polarimetry can help mitigate this, though the analysis remains difficult due to the typically very low degree of polarization, even for hot Jupiters, unlike binary stars, where polarization is more pronounced. In a planetary atmosphere (if present), starlight is scattered by gas molecules, aerosols, and/or cloud particles, and may also reflect off the surface if the atmosphere is not optically thick. Each scattering interaction modifies the outgoing radiation, affecting both the degree and direction of polarization seen in the observed Stokes q and u parameters.

 $\upsilon$  And b, a well-known hot Jupiter, is the innermost planet in the Upsilon Andromedae system. It has an orbital period of just over 4.6 d and a mass of about 1.7  $M_{\rm J}$  (Piskorz et al., 2017). It was among the earliest exoplanets discovered via Doppler spectroscopy (Butler et al., 1997). The host star is an F8 dwarf with three additional known planets (McArthur et al., 2010). As a non-transiting planet,  $\upsilon$  And b's orbital parameters, such as inclination can potentially be revealed through polarimetry, which other techniques cannot achieve. Due to its size and favorable sky position,  $\upsilon$  And b has been considered one of the most promising targets expected to exhibit a detectable polarization signal dominated by Rayleigh scattering.

### 5.1 Data Observations

We observed v And during 114 nights from 2016 to 2019 using DiPol-2 polarimeter installed at the remotely controlled T60 telescope at Haleakalā Observatory, Hawaii, USA. The host star of the planetary system v And is a bright target with an apparent

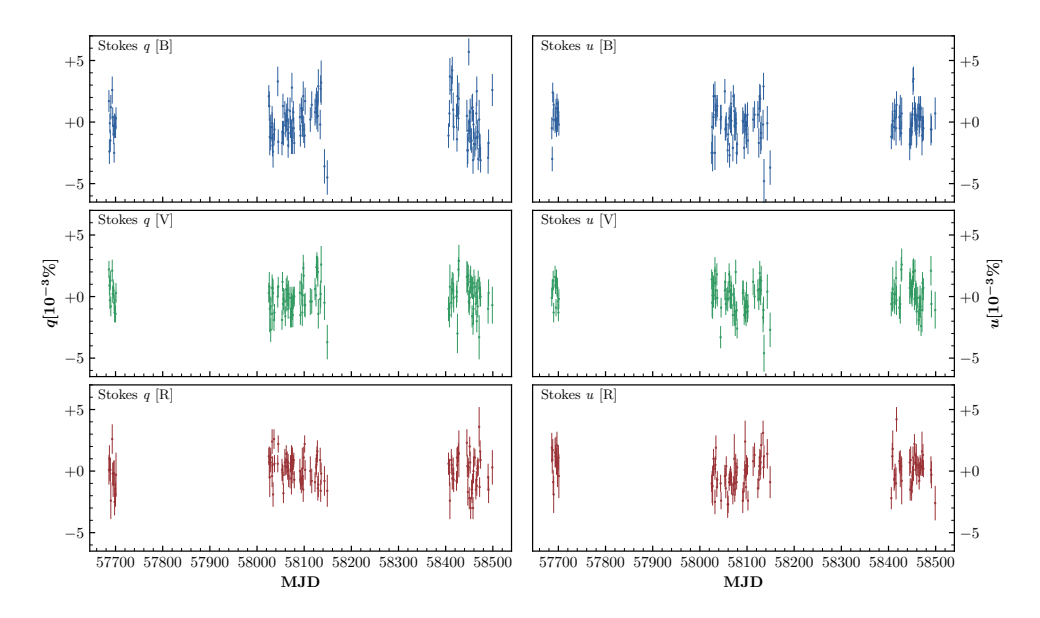


**Figure 7.** De-trended observations of Stokes q (left panels) and u (right panels) observations in B (top panels), V (middle panels), and R (bottom panels) passbands with  $\pm \sigma$  uncertainties for v And, measured from 2016 October to 2019 January (MJD 57686–58499).

magnitude of 4.60 and thus visible to the human eye. At the Haleakalā summit,  $\upsilon$  And is well visible from September through March. Skyflat images that are used for calibration purposes were regularly taken at the time of twilight hours, either at the beginning of the observing night or at dawn. Once per night, the series of dark and bias images were also taken.

Telescope instrumental polarization was derived from observations of 15–20 zero-polarized standard stars. It was found to be in the range of 0.004%-0.006% and it was measured in each passband with the accuracy at least of  $5\sigma$ . To determine the polarization angle zero-point, observations of highly polarized standard stars were made. In general, for determination of the intrinsic polarization of the distant object, the interstellar polarization should be measured and subtracted. It is normally done by observing a few objects in the vicinity of the target. However, because v And is located at the distance of only 13.5 pc from the Sun (Gaia Collaboration et al., 2021), the contribution from interstellar polarization component should be  $\ll 10^{-4}$  (e.g., Piirola et al. (2021)). This component of polarization, even if it exists, must be constant with time and thus introduce only permanent offset in the observed Stokes parameters.

The calibrated polarization data for v And b in B, V, and R passbands are shown in Fig. 7 as variations of the Stokes parameters q and u with time. We noticed slight trends in Stokes q and u between different observing seasons, likely due to the long duration of our data set, which is common in extended time-series observations. To

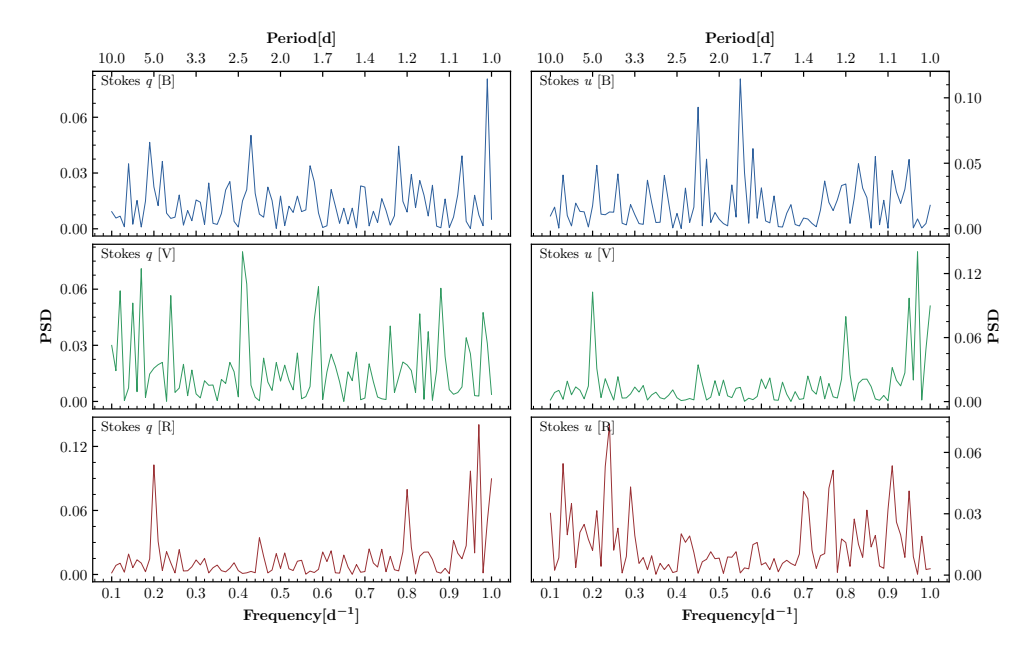


**Figure 8.** Lomb-Scargle periodograms for Stokes q (left column) and u (right column) of v And in B, V, and R passbands (top, middle, and bottom panels respectively).

mitigate these effects, we applied a de-trending procedure. The timescale of this de-trending is significantly longer than the orbital period of the exoplanet, ensuring that the process removes only long-term instrumental or systematic trends without affecting the orbital polarization signal.

### 5.2 Period Search

To determine periodic signals in the polarimetric data of v And b, we employed the LS algorithm. LS periodograms for both Stokes q and u in the B, V, and R passbands are shown in Fig. 8. At first glance, the periodograms appear noisy, which is not surprising, given the sensitivity of the polarimeter compared to the degree of intrinsic polarization variations predicted for hot Jupiters by various models. A closer inspection, however, reveals peaks in the Lomb–Scargle periodograms at around 2.3 d, half of the known orbital period of v And b, for Stokes q in the B and R passbands and for Stokes u in the B passband only. However, such peaks in the other passbands, if present, have low power spectral density (PSD). These periodograms also exhibit multiple stronger peaks at other frequencies. The peaks at around 1.0 d may result from the regular nightly observation cadence.

Even though the presence of peaks around half of the planetary orbital period of v And b can be observed in most periodograms, peaks at around 1.8 d are also noticeable. These are most likely alias peaks produced by the periodicity in the

observation timings coupled with the periodic nature of the source. As explained in the previous chapter, if the signal period is not less than half the sampling frequency (i.e., the Nyquist frequency,  $f_{\rm ny}$ ), a side effect can occur, producing two signals that differ by  $1/f_{\rm ny}$ . A (half) orbital period of v And b, ~2.3 d, corresponds to a frequency of 0.43 d<sup>-1</sup>, which is indeed more than half the sampling frequency since we observed approximately once per night. Therefore, an alias peak can be expected at  $1/(1-1/2.3)=1.76\,{\rm d}$ , which is precisely where the periodograms show the alias peaks. A possible, though impractical, solution would be to observe v And b twice per day to overcome the Nyquist criterion and eliminate aliasing in the periodograms.

Furthermore, we examined the FAPs of the planetary orbital peaks in the periodograms of the original data (see Fig. 8). For Stokes q data, the FAP values are 35% at a frequency of 0.43 d<sup>-1</sup> (~2.3 d) in the B band, 43% at 0.42 d<sup>-1</sup> (~2.4 d) in the V band, and 99% at 0.43 d<sup>-1</sup> (~2.3 d) in the R band. For Stokes u, the values are 47% at 0.45 d<sup>-1</sup> (~2.2 d) in the B band, 66% at 0.43 d<sup>-1</sup> (~2.3 d) in the V band, and 99% at 0.43 d<sup>-1</sup> (~2.3 d) in the R band. The false alarm probability (FAP) values may seem quite high, but considering the noisy nature of our polarimetric data, we believe that in the B and V passbands, a real signal at peaks between 2.2 and 2.4 d i.e., around half the known orbital period of v And b, corresponding to greater than 50% probability, cannot be entirely ruled out.

### 5.3 RL Approximation

Polarization measurements of exoplanets offer a unique insight into the physical properties of their atmospheres and the scattering processes that occur as starlight interacts with them. In particular, understanding how polarization varies with the orbital phase of an exoplanet provides important constraints on the geometry of the exoplanet system, including the inclination, orbital parameters, and scattering characteristics of the planet's atmosphere. In this framework, we can model the polarization arising from an exoplanet in a circular orbit. We assume that the exoplanet's atmosphere behaves as a Lambertian scatterer, and the polarization follows the same scattering angle dependence as Rayleigh scattering. This approach allows us to derive a functional form for the polarization as a function of orbital phase, which can be used to compare with observational data.

Let us now consider a basic model of polarization arising from an exoplanet in a circular orbit. In this scenario, we assume a Lambertian phase function and polarization due to scattering in the planetary atmosphere, with the scattering angle behaving similarly to Rayleigh scattering. This model can be mathematically described as (Seager et al., 2000; Wiktorowicz, 2009):

$$P(\phi) = \epsilon F(\phi) P_0(\phi), \tag{55}$$

where  $\phi$  is the orbital phase ( $\phi = 0$  indicates the superior conjunction of the exo-

planet),  $F(\phi)$  is the phase function,  $P_0(\phi)$  is the polarization of scattered flux, and  $\epsilon$  represents the fraction of stellar flux scattered by the planet:

$$\epsilon = p(R_{\rm RL}/a)^2,\tag{56}$$

where  $R_{\rm RL}$  is the RL radius (i.e., the effective scattering radius of the planet), a is the semi-major axis of the planetary orbit and p is the geometric albedo, representing the fraction of exoplanetary scattered flux at full phase compared to that scattered by a Lambertian disk. For a Lambertian disk, p=2/3 (Wiktorowicz, 2009). The fraction of the solid angle occupied by the planet, as seen from the star, is  $\pi R_{\rm RL}^2/4\pi a^2$ , so the value of p is multiplied by 1/4. The analytical form of the phase function in terms of the phase angle  $\alpha$  (the angle between the host star and the observer as seen from the exoplanet) is given by Russell (1916):

$$F(\alpha) = \frac{\sin \alpha + (\pi - \alpha)\cos \alpha}{\pi}.$$
 (57)

Substituting  $\cos \alpha = \sin i \cos \phi$ , where i is the inclination angle, we can express F as a function of  $\phi$ . Moreover, we can express  $P(\phi)$  as:

$$P(\phi) = \sqrt{q^2(\phi) + u^2(\phi)},\tag{58}$$

where  $q(\phi)$  and  $u(\phi)$  are normalized Stokes parameters. In the orbital frame, Stokes  $q'(\phi)$  and  $u'(\phi)$  are described by Shakhovskoi (1965):

$$q'(\phi) = \epsilon F(\alpha) \left(\sin^2 \phi - \cos^2 \phi \cos^2 i\right), \tag{59}$$

$$u'(\phi) = \epsilon F(\alpha) \sin 2\phi \cos i. \tag{60}$$

In order to convert Stokes  $q'(\phi)$  and  $u'(\phi)$  from the orbital frame to celestial coordinates, we need to find the rotation angle from the longitude of the ascending node  $\Omega$ . This angle is  $\theta = \Omega + 270^{\circ}$ , and we obtain (Chandrasekhar, 1960; Wiktorowicz, 2009):

$$q(\phi) = q'(\phi)\cos 2\theta - u'(\phi)\sin 2\theta, \tag{61}$$

$$u(\phi) = q'(\phi)\sin 2\theta + u'(\phi)\cos 2\theta. \tag{62}$$

Furthermore,  $\phi=l+\omega$  and  $l=(2\pi/P_{\rm orb})(t-T_0)$ , where  $P_{\rm orb}$  is the orbital period, t is the time of observation, and  $T_0$  is the periastron epoch. The polarimetric data were modeled using Eq. (61) and (62), where constant offsets  $Z_{\rm q}$  and  $Z_{\rm u}$  were added to  $q(\phi)$  and  $u(\phi)$ , respectively, to account for constant intrinsic/interstellar polarization. The free parameters of the model are the inclination angle i, the argument of periastron  $\omega$ , the longitude of the ascending node  $\Omega$ , the geometric albedo p, and the offsets  $Z_{\rm q}$  and  $Z_{\rm u}$ .

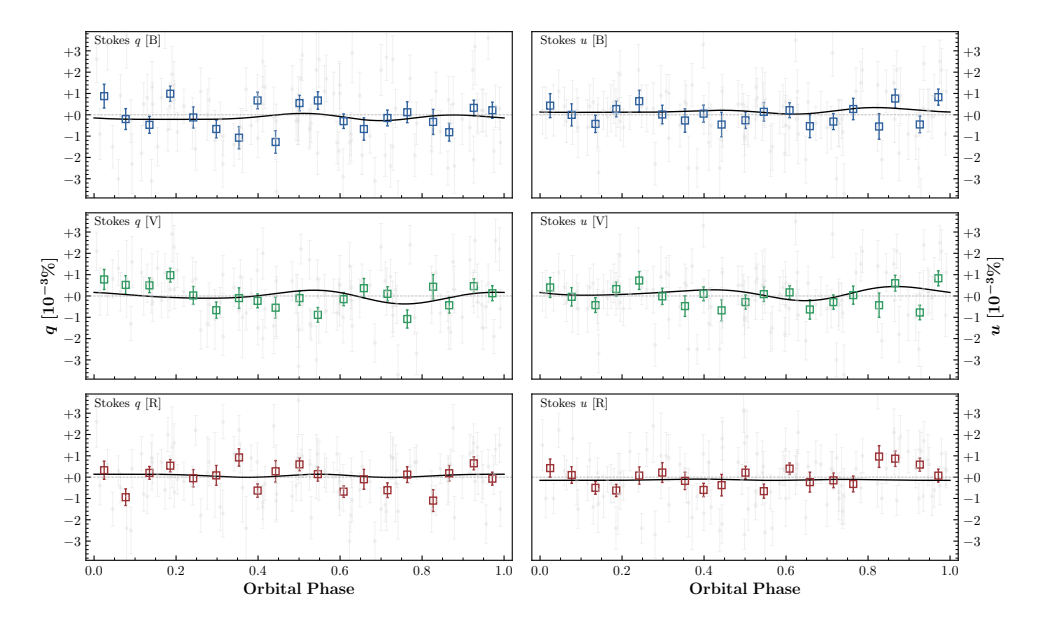


**Figure 9.** The variability of Stokes q (left column) and u (right column) of v And b in B, V, and R passbands (from top to bottom), phase-folded at the orbital period of 4.62 d. The squares are the data points with error bars that correspond to the average values of the individual observations (light gray circles with error bars) and the standard errors of the mean calculated for the orbital phase bin size of 0.053. The black solid lines correspond to the best-fit obtained using RL approximation with  $\chi^2$  minimization. Phase 0.0 corresponds to periastron epoch.

This model is a critical tool for interpreting polarimetric observations of exoplanets, allowing us to extract important information about their orbital parameters and scattering properties. By comparing the model to observational data, we can test the validity of assumptions about planetary atmospheres and refine our understanding of the factors influencing exoplanet polarization.

### 5.4 Results and Discussion

In order to deduce orbital parameters by RL approximation, we phase-folded the data for Stokes q and u parameters in the B, V, and R passbands. The ephemeris used was  $T_0=2450034.058\pm0.3$  JD and the orbital period of  $P=4.61711\pm0.00018$  d, given by Deitrick et al. (2015). Furthermore, the data was binned at an orbital phase interval of 0.053 by using data uncertainties as inverse square error to weigh the individual data points. This procedure helped reduce the noise and made the periodic variability more prominent. The orbital parameters such as  $i, \omega, \Omega$ , and p are independent of wavelength and ideally the data of all three passbands should be fitted simultaneously. However, in the case of Rayleigh scattering the amplitude of polarization should drop with the wavelength. Therefore, we opted to fit the data

Parameter	В	V	R
$R_{\rm RL} [R_{\rm J}]^{(a)}$		1.6	
$i [\deg]^{(b)}$	$72^{+26}_{-38}$	$28^{+88}_{-18}$	$87  ^{+30}_{-46}$
$\omega  [\deg]^{(b)}$	$117^{+69}_{-80}$	$102^{+139}_{-45}$	$162^{+90}_{-104}$
$\Omega  [\text{deg}]^{(\text{b})}$	$105^{+68}_{-85}$	$107^{+134}_{-43}$	$171^{+139}_{-126}$
$p \ [\%]^{(b)}$	$16^{+17}_{-8}$	$19^{+9}_{-8}$	$9^{+12}_{-5}$
$Z_{\mathrm{q}}~[\%]^{(\mathrm{b})}$	$0.000214_{-0.000218}^{+0.000129}$	$0.000003^{+0.000077}_{-0.000112}$	$-0.000137 {}^{+0.000281}_{-0.000087}$
$Z_{\mathrm{u}} \ [\%]^{(\mathrm{b})}$	$-0.000116^{+0.000164}_{-0.000092}$	$-0.000123_{-0.000124}^{+0.000079}$	$0.000150^{+0.000076}_{-0.000252}$
$\chi^2$ /d.o.f.	466/222	412/222	423/222

**Table 1.** Best-fit orbital parameters for v And b.

of each passband separately. The polarimetric observations measure a combination of the geometric albedo and planet area:  $p(R_{\rm RL}/a)^2$ , where  $R_{\rm RL}$  is planetary radius, and a is semi-major axis. Therefore, in order to deduce either p or  $R_{\rm RL}$ , one of the parameters must be known. For our fits, we adopted a radius of  $1.6\,R_{\rm J}$  for v And b as a reasonable midpoint between the  $1.3\,R_{\rm J}$  assumed by Crossfield et al. (2010) and the  $\sim 1.8\,R_{\rm J}$  suggested by Deitrick et al. (2015).

Figure 9 shows the best-fit curves for the Stokes q and u parameters in the B, V, and R passbands using the RL approximation. The fits are poor overall, with low peak-to-peak amplitudes and significant scatter in the binned data. The R-band results are particularly weak, with best-fit curves appearing nearly flat. Confidence intervals for the fitted orbital parameters are broad across all passbands, rendering the derived values unreliable. Despite detecting phase-locked polarization variability, especially in B and V bands, the noise level prevents meaningful orbital parameter extraction. As shown in Table 1, the fitted orbital inclinations for B and R bands,  $72^{+26\circ}_{-38}$  and  $87^{+30\circ}_{-46}$  respectively, are inconsistent with the known non-transiting nature of v And b. Only the V band yields a plausible value,  $28^{+88\circ}_{-18}$ , which overlaps with the previously reported  $24^{\circ} \pm 4^{\circ}$  by Piskorz et al. (2017). However, the uncertainties remain too large to draw firm conclusions.

The wide confidence intervals reflect limitations from both data quality and residual systematics. Our V-band values for the argument of periastron,  $\omega=102^{+139\circ}_{-45}$ , and longitude of the ascending node,  $\Omega=107^{+134\circ}_{-43}$ , differ from previous findings. For example, McArthur et al. (2010) report  $\omega=44\pm26^\circ$ , and Curiel et al. (2011) find  $\omega=324.3\pm3.8^\circ$ . Our result aligns better with Butler et al. (1997), who found 63°, though uncertainties remain large. The value of  $\Omega$  is consistent with the 180°

<sup>(</sup>a) Fixed parameter. (b) Uncertainties represent 16th/84th percentiles (equivalent to  $\pm 1\sigma$ ).

ambiguity inherent to polarimetric measurements (Drissen et al., 1986), making it broadly compatible with our derived value of  $256^{+12}_{-17}$ °. The retrieved parameters may contain a genuine polarimetric signal despite the noise, but this cannot be asserted with certainty. Our derived values of geometric albedo p are low across all bands, likely reflecting data limitations and possible contamination from stellar activity. In the absence of prior constraints, we refrain from definitive claims about v And b's geometric albedo.

Several strategies for improved data were considered. A follow-up dataset was acquired with DiPol-2 on the 1 m Calern telescope in France, but poor weather reduced its quality. Future prospects may include increasing nightly integration time from 1.5 to 6 hours, though such extended observations are currently impractical. We can identify two major obstacles in detecting polarization signals from exoplanets. i) Accuracy much better than few parts per million is necessary and this can only be achieved by collecting more than  $10^{12}$  photons. To collect such number, total integration times even for the few known brightest exoplanets become unrealistically long even when large telescopes are employed, ii) At the polarization signal level of  $10^{-6}$ , polarization effects related to star surface spots become significant and must be somehow taken into account.

Ultimately, space-based polarimetry with large telescopes and advanced photon detectors may be required to robustly determine the orbital parameters of hot Jupiters like  $\upsilon$  And b.

### 6 Conclusions

This dissertation presents a comprehensive study on the application of high-precision broadband linear polarimetry to early-type binary star systems and an exoplanet. The research primarily focuses on deriving orbital parameters, estimating ISP, and exploring the physical properties of these systems through phase-locked polarization variability. The findings contribute to a deeper understanding of their geometry, dynamics, and evolution.

We primarily used the DiPol-2 polarimeter in combination with the T60 telescope to perform high-precision broadband optical polarization measurements. Our broadband (B, V, and R passbands) linear polarimetric observations included the O+O binary star systems AO Cas, DH Cep, and HD 165052, as well as the well-known X-ray binary system Hercules X-1 (Her X-1) in optical wavelengths. Additionally, we observed the Algol-type binaries AS Eridani (AS Eri), and RZ Cassiopeiae (RZ Cas), along with the variable star PZ Geminorum (PZ Gem). Finally, we conducted long-term observations of two hot Jupiters:  $\upsilon$  And b and Tau Boötis b ( $\tau$  Boö b).

For the binary star systems, we derived orbital inclinations and longitudes of the ascending node for AO Cas, DH Cep, and HD 165052 using the BME method. Our results provided insights into the geometry and dynamics of these systems, with polarization variability primarily driven by Thomson scattering in the circumstellar environment. The polarization amplitude and phase curves were well-fitted by the BME model, revealing a symmetric distribution of scattering material around the binary components. For AO Cas, our results were consistent with polarimetric studies conducted over half a century ago. As we have found, the light scattering geometry in this system remains stable over this period of time. We conducted the first comprehensive polarimetric study of DH Cep, which, resulted in detection of phase-locked variable linear polarization with total amplitude of  $\simeq 0.2\%$ . Our findings aligned well with those obtained through other observational techniques. By observing stars in the open cluster NGC 7380, where DH Cep resides, we confirmed the cluster's uniform dust distribution as indicated by previous studies. Furthermore, we estimated the mass-loss rate of DH Cep using polarimetry, a novel achievement for an O+O system. For HD 165052 our observations resulted in discovery of phaselocked variable polarization with peak-to-peak amplitude  $\leq 0.2\%$ . Our period search allowed us to rectify the orbital period value and showed that recently determined period value obtained from RV measurements by Rosu et al. (2023) is too long. The

low binary inclination of HD 165052 ( $\sim\!45^\circ$ ) prevented us from deriving an accurate orbit inclination angle, which is expected from applying the BME method. However, we successfully estimated the mass-loss rates of the individual components, which were in agreement with results from other techniques. Accurate ISP estimation was achieved for AO Cas and DH Cep by observing nearby field stars, although this was not possible for HD 165052 due to the cluster's young age and non-uniform dust distribution.

For the exoplanet  $\upsilon$  And b, we detected a periodic signal in our polarimetric data. However, deriving precise orbital and physical parameters using the Rayleigh-Lambert (RL) approximation proved challenging due to the weak and noisy signal. Subsequent observations with the larger 1-meter Calern telescope did not improve data quality. We were able to derive somewhat reasonable estimates in the V passband, albeit with high uncertainties. Overcoming this limitation may require even larger telescopes or space-based polarimetric observations to eliminate atmospheric contamination.

The unpublished work includes observations of Her X-1, AS Eri, RZ Cas, PZ Gem, and  $\tau$  Boö b. Further analysis was not pursued because the polarimetric data exhibited no clear periodic signals. Any potential polarization signals from these targets were likely too weak to be modeled accurately.

The findings of this dissertation have significant implications for astrophysics, particularly in the study of binary star systems and exoplanets. The derived orbital parameters and mass-loss rates offer valuable constraints for theoretical models of binary star evolution, especially in systems with strong stellar winds and mass transfer. Polarization variability provides a powerful diagnostic tool for probing the geometry and dynamics of circumstellar environments. Additionally, our work emphasizes the role of dust distribution in shaping polarization patterns, with broader implications for understanding the evolutionary stages of star clusters and the interactions between stars and the interstellar medium.

Looking ahead, several avenues for future research remain. Expanding the sample of binary star systems to include those with diverse spectral types, orbital configurations, and evolutionary stages could provide a more comprehensive understanding of polarization's role in probing binary interactions and circumstellar environments. Studying systems with eccentric orbits or asymmetric scattering geometries may reveal new insights into the dynamics of mass transfer and stellar winds. Advancements in exoplanet polarimetry, including the development of more sensitive instruments, could improve measurement precision and yield more accurate results.

In conclusion, this dissertation demonstrates the power of high-precision broadband optical linear polarimetry as a diagnostic tool for studying binary star systems and exoplanets exhibiting phase-locked polarization variability. The research presented here advances our understanding of the geometry, dynamics, and evolution of these systems while laying the foundation for future studies. As observational techniques and theoretical models continue to evolve, polarimetry will play an increasingly critical role in addressing fundamental questions in astrophysics, paving the way for new discoveries and a deeper understanding of the universe.

### List of References

- Abdul Qadir, Y., Berdyugin, A. V., Piirola, V., Sakanoi, T., and Kagitani, M. (2023a). High-precision broadband linear polarimetry of early-type binaries. III. AO Cassiopeiae revisited. *A&A*, 670:A176.
- Abdul Qadir, Y., Berdyugin, A. V., Piirola, V., Sakanoi, T., and Kagitani, M. (2023b). High-precision broadband linear polarimetry of early-type binaries. IV. The DH Cephei binary system in the open cluster of NGC 7380. *A&A*, 677:A75.
- Abdul Qadir, Y., Berdyugin, A. V., Piirola, V., Sakanoi, T., Kagitani, M., and Berdyugina, S. V. (2025). High-precision broadband linear polarimetry of early-type binaries: V. The binary system HD 165052 in the open cluster NGC 6530. *A&A*, 697:A133.
- Andersson, B. G., Lazarian, A., and Vaillancourt, J. E. (2015). Interstellar Dust Grain Alignment. *ARA&A*, 53:501–539.
- Aspin, C., Simmons, J. F. L., and Brown, J. C. (1981). Polarimetric Accuracy Required for the Determination of Binary Inclinations. *MNRAS*, 194:283.
- Axon, D. J. and Ellis, R. S. (1976). A catalogue of linear polarization measurements for 5070 stars. *MNRAS*, 177:499.
- Bailey, J., Kedziora-Chudczer, L., and Bott, K. (2018). Polarized radiative transfer in planetary atmospheres and the polarization of exoplanets. *MNRAS*, 480(2):1613–1625.
- Berdyugin, A., Piirola, V., and Poutanen, J. (2019). High-precision optical polarimetry. In Mignani, R., Shearer, A., Słowikowska, A., and Zane, S., editors, *Astronomical Polarisation from the Infrared to Gamma Rays*, volume 460 of *Astrophysics and Space Science Library*, pages 119–144. Springer Nature, Cambridge, UK.
- Berdyugin, A., Piirola, V., Sadegi, S., Tsygankov, S., Sakanoi, T., Kagitani, M., Yoneda, M., Okano, S., and Poutanen, J. (2016). High-precision broad-band linear polarimetry of early-type binaries. I. Discovery of variable, phase-locked polarization in HD 48099. *A&A*, 591:A92.
- Berdyugina, S. V., Berdyugin, A. V., Fluri, D. M., and Piirola, V. (2008). First Detection of Polarized Scattered Light from an Exoplanetary Atmosphere. *ApJ*, 673(1):L83.
- Berdyugina, S. V., Berdyugin, A. V., Fluri, D. M., and Piirola, V. (2011). Polarized Reflected Light from the Exoplanet HD189733b: First Multicolor Observations and Confirmation of Detection. *ApJ*, 728(1):L6.
- Bohren, C. F. and Albrecht, B. A. (1998). *Atmospheric Thermodynamics*. Oxford University Press, Oxford.
- Born, M. and Wolf, E. (1959). *Principles of Optics: Electromagnetic Theory of Propagation, Interference and Diffraction of Light*. Pergamon Press, Oxford.
- Bott, K., Bailey, J., Kedziora-Chudczer, L., Cotton, D., and Marshall, J. (2016). Polarimetry of hot-Jupiter systems and radiative transfer models of planetary atmospheres. In *American Astronomical Society Meeting Abstracts* #227, page 112.02.
- Breger, M. (1982). Polarization in NGC 7789 and the membership of blue stragglers. *ApJ*, 263:199–206.

- Breger, M. (1986). The Pleiades Cluster. III. Polarization, Reddening, and the Unusual Distribution of Interstellar Matter. *ApJ*, 309:311.
- Brown, J. C. and McLean, I. S. (1977). Polarisation by Thomson Scattering in Optically Thin Stellar Envelopes. I. Source Star at Centre of Axisymmetric Envelope. *A&A*, 57:141.
- Brown, J. C., McLean, I. S., and Emslie, A. G. (1978). Polarisation by Thomson scattering in optically thin stellar envelopes. II. Binary and multiple star envelopes and the determination of binary inclinations. *A&A*, 68:415–427.
- Butler, R. P., Marcy, G. W., Williams, E., Hauser, H., and Shirts, P. (1997). Three New "51 Pegasi-Type" Planets. *ApJ*, 474(2):L115–L118.
- Carciofi, A. C. and Magalhães, A. M. (2005). The Polarization Signature of Extrasolar Planet Transiting Cool Dwarfs. *ApJ*, 635(1):570–577.
- Cardelli, J. A., Clayton, G. C., and Mathis, J. S. (1989). The relationship between IR, optical, and UV extinction. In Allamandola, L. J. and Tielens, A. G. G. M., editors, *Interstellar Dust*, volume 135 of *IAU Symposium*, pages 5–10.
- Chandrasekhar, S. (1946). On the Radiative Equilibrium of a Stellar Atmosphere. X. *ApJ*, 103:351.
- Chandrasekhar, S. (1960). Radiative Transfer. Dover Publications, New York.
- Clarke, D. (2010). Stellar Polarimetry. Wiley, Chichester.
- Coyne, G. V. and Gehrels, T. (1966). Wavelength dependence of polarization. VIII. Interstellar polarization. *AJ*, 71:355–363.
- Crossfield, I. J. M., Hansen, B. M. S., Harrington, J., Cho, J. Y. K., Deming, D., Menou, K., and Seager, S. (2010). A New 24  $\mu$ m Phase Curve for v Andromedae b. ApJ, 723(2):1436–1446.
- Curiel, S., Cantó, J., Georgiev, L., Chávez, C. E., and Poveda, A. (2011). A fourth planet orbiting v Andromedae. A&A, 525:A78.
- Davis, Jr., L. and Greenstein, J. L. (1951). The Polarization of Starlight by Aligned Dust Grains. *ApJ*, 114:206.
- de Bruyn, G. and Brentjens, M. A. (2005). Deep WSRT 0.35-1.4 GHz imaging of the Perseus cluster. *Highlights of Astronomy*, 13:331.
- Deitrick, R., Barnes, R., McArthur, B., Quinn, T. R., Luger, R., Antonsen, A., and Benedict, G. F. (2015). The Three-dimensional Architecture of the  $\upsilon$  Andromedae Planetary System. *ApJ*, 798(1):46.
- Dolginov, A. Z. and Mitrofanov, I. G. (1976). Orientation of Cosmic Dust Grains. *Ap&SS*, 43(2):291–317.
- Donati, J. F., Semel, M., Carter, B. D., Rees, D. E., and Collier Cameron, A. (1997). Spectropolarimetric observations of active stars. *MNRAS*, 291(4):658–682.
- Draine, B. T. and Weingartner, J. C. (1996). Radiative Torques on Interstellar Grains. I. Superthermal Spin-up. *ApJ*, 470:551.
- Draine, B. T. and Weingartner, J. C. (1997). Radiative Torques on Interstellar Grains. II. Grain Alignment. *ApJ*, 480(2):633–646.
- Drissen, L., Lamontagne, R., Moffat, A. F. J., Bastien, P., and Seguin, M. (1986). Spectroscopic and Polarimetric Parameters of the Runaway WN7 Binary System HD 197406: Is the Secondary an X-Ray–quiet Black Hole? *ApJ*, 304:188.
- Eswaraiah, C., Pandey, A. K., Maheswar, G., Medhi, B. J., Pandey, J. C., Ojha, D. K., and Chen, W. P. (2011). A multiwavelength polarimetric study towards the open cluster NGC 1893. *MNRAS*, 411(3):1418–1434.
- Feinstein, C., Vergne, M. M., Martínez, R., and Orsatti, A. M. (2008). Optical polarization

study in the open cluster NGC 6250. MNRAS, 391(1):447-456.

Fluri, D. M. and Berdyugina, S. V. (2010). Orbital parameters of extrasolar planets derived from polarimetry. *A&A*, 512:A59.

Forsblom, S. V., Tsygankov, S. S., Poutanen, J., Doroshenko, V., Mushtukov, A. A., Ng, M., Ravi, S., Marshall, H. L., Di Marco, A., La Monaca, F., Malacaria, C., Mastroserio, G., Loktev, V., Possenti, A., Suleimanov, V. F., Taverna, R., Agudo, I., Antonelli, L. A., Bachetti, M., Baldini, L., Baumgartner, W. H., Bellazzini, R., Bianchi, S., Bongiorno, S. D., Bonino, R., Brez, A., Bucciantini, N., Capitanio, F., Castellano, S., Cavazzuti, E., Chen, C.-T., Ciprini, S., Costa, E., De Rosa, A., Del Monte, E., Di Gesu, L., Di Lalla, N., Donnarumma, I., Dovčiak, M., Ehlert, S. R., Enoto, T., Evangelista, Y., Fabiani, S., Ferrazzoli, R., Garcia, J. A., Gunji, S., Hayashida, K., Heyl, J., Iwakiri, W., Jorstad, S. G., Kaaret, P., Karas, V., Kislat, F., Kitaguchi, T., Kolodziejczak, J. J., Krawczynski, H., Latronico, L., Liodakis, I., Maldera, S., Manfreda, A., Marin, F., Marinucci, A., Marscher, A. P., Massaro, F., Matt, G., Mitsuishi, I., Mizuno, T., Muleri, F., Negro, M., Ng, C.-Y., O'Dell, S. L., Omodei, N., Oppedisano, C., Papitto, A., Pavlov, G. G., Peirson, A. L., Perri, M., Pesce-Rollins, M., Petrucci, P.-O., Pilia, M., Puccetti, S., Ramsey, B. D., Rankin, J., Ratheesh, A., Roberts, O. J., Romani, R. W., Sgrò, C., Slane, P., Soffitta, P., Spandre, G., Swartz, D. A., Tamagawa, T., Tavecchio, F., Tawara, Y., Tennant, A. F., Thomas, N. E., Tombesi, F., Trois, A., Turolla, R., Vink, J., Weisskopf, M. C., Wu, K., Xie, F., and Zane, S. (2024). Probing the polarized emission from SMC X-1: The brightest X-ray pulsar observed by IXPE. A&A, 691:A216.

Fresnel, A.-J. (1821). Mémoire sur la théorie de la lumière. *Mémoires de l'Académie des Sciences de l'Institut de France*, 5.

Gaia Collaboration, Brown, A. G. A., Vallenari, A., Prusti, T., de Bruijne, J. H. J., Babusiaux, C., Biermann, M., Creevey, O. L., Evans, D. W., Eyer, L., Hutton, A., Jansen, F., Jordi, C., Klioner, S. A., Lammers, U., Lindegren, L., Luri, X., Mignard, F., Panem, C., Pourbaix, D., Randich, S., Sartoretti, P., Soubiran, C., Walton, N. A., Arenou, F., Bailer-Jones, C. A. L., Bastian, U., Cropper, M., Drimmel, R., Katz, D., Lattanzi, M. G., van Leeuwen, F., Bakker, J., Cacciari, C., Castañeda, J., De Angeli, F., Ducourant, C., Fabricius, C., Fouesneau, M., Frémat, Y., Guerra, R., Guerrier, A., Guiraud, J., Jean-Antoine Piccolo, A., Masana, E., Messineo, R., Mowlavi, N., Nicolas, C., Nienartowicz, K., Pailler, F., Panuzzo, P., Riclet, F., Roux, W., Seabroke, G. M., Sordo, R., Tanga, P., Thévenin, F., Gracia-Abril, G., Portell, J., Teyssier, D., Altmann, M., Andrae, R., Bellas-Velidis, I., Benson, K., Berthier, J., Blomme, R., Brugaletta, E., Burgess, P. W., Busso, G., Carry, B., Cellino, A., Cheek, N., Clementini, G., Damerdji, Y., Davidson, M., Delchambre, L., Dell'Oro, A., Fernández-Hernández, J., Galluccio, L., García-Lario, P., Garcia-Reinaldos, M., González-Núñez, J., Gosset, E., Haigron, R., Halbwachs, J. L., Hambly, N. C., Harrison, D. L., Hatzidimitriou, D., Heiter, U., Hernández, J., Hestroffer, D., Hodgkin, S. T., Holl, B., Janßen, K., Jevardat de Fombelle, G., Jordan, S., Krone-Martins, A., Lanzafame, A. C., Löffler, W., Lorca, A., Manteiga, M., Marchal, O., Marrese, P. M., Moitinho, A., Mora, A., Muinonen, K., Osborne, P., Pancino, E., Pauwels, T., Petit, J. M., Recio-Blanco, A., Richards, P. J., Riello, M., Rimoldini, L., Robin, A. C., Roegiers, T., Rybizki, J., Sarro, L. M., Siopis, C., Smith, M., Sozzetti, A., Ulla, A., Utrilla, E., van Leeuwen, M., van Reeven, W., Abbas, U., Abreu Aramburu, A., Accart, S., Aerts, C., Aguado, J. J., Ajaj, M., Altavilla, G., Álvarez, M. A., Álvarez Cid-Fuentes, J., Alves, J., Anderson, R. I., Anglada Varela, E., Antoja, T., Audard, M., Baines, D., Baker, S. G., Balaguer-Núñez, L., Balbinot, E., Balog, Z.,

- Barache, C., Barbato, D., Barros, M., Barstow, M. A., Bartolomé, S., Bassilana, J. L., Bauchet, N., Baudesson-Stella, A., Becciani, U., Bellazzini, M., Bernet, M., Bertone, S., Bianchi, L., Blanco-Cuaresma, S., Boch, T., Bombrun, A., Bossini, D., Bouquillon, S., Bragaglia, A., Bramante, L., Breedt, E., Bressan, A., Brouillet, N., Bucciarelli, B., Burlacu, A., Busonero, D., Butkevich, A. G., Buzzi, R., Caffau, E., Cancelliere, R., Cánovas, H., Cantat-Gaudin, T., Carballo, R., Carlucci, T., Carnerero, M. I., Carrasco, J. M., Casamiquela, L., Castellani, M., Castro-Ginard, A., Castro Sampol, P., Chaoul, L., Charlot, P., Chemin, L., Chiavassa, A., Cioni, M. R. L., Comoretto, G., Cooper, W. J., Cornez, T., Cowell, S., Crifo, F., Crosta, M., Crowley, C., Dafonte, C., Dapergolas, A., David, M., and David, P. (2021). Gaia Early Data Release 3. Summary of the contents and survey properties (Corrigendum). *A&A*, 650:C3.
- Goldstein, D. (2003). Polarized Light. Marcel Dekker, New York.
- Goodman, A. A., Bastien, P., Myers, P. C., and Menard, F. (1990). Optical Polarization Maps of Star-forming Regions in Perseus, Taurus, and Ophiuchus. *ApJ*, 359:363.
- Hall, J. S. (1949). Observations of the Polarized Light from Stars. *Science*, 109(2825):166–167.
- Harries, T. J., Hillier, D. J., and Howarth, I. D. (1998). A spectropolarimetric survey of northern hemisphere Wolf-Rayet stars. *MNRAS*, 296(4):1072–1088.
- Harrington, J. P. (1970). Polarization of Radiation from Stellar Atmospheres. The Grey Case. *Ap&SS*, 8(2):227–242.
- Harrington, J. P. and Collins, II, G. W. (1968). Intrinsic Polarization of Rapidly Rotating Early-Type Stars. *ApJ*, 151:1051.
- Heaviside, O. (1885). *Electromagnetic Theory*. The Electrician Printing and Publishing Company, London.
- Hecht, E. (2017). Optics. Pearson Education, Boston.
- Hiltner, W. A. (1947). On the Presence of Polarization in the Continuous Radiation of Early-Type Stars. *ApJ*, 106:231.
- Hiltner, W. A. (1949). Polarization of Radiation from Distant Stars by the Interstellar Medium. *Nature*, 163(4138):283.
- Hiltner, W. A. (1956). Photometric, Polarization, and Spectrographic Observations of O and B Stars. *ApJS*, 2:389.
- Hough, J. (2006). Polarimetry: a powerful diagnostic tool in astronomy. *Astronomy and Geophysics*, 47(3):3.31–3.35.
- Hough, J., Lucas, P. W., and Bailey, J. (2006). The polarization signature of extra-solar planets. In Whitelock, P., Dennefeld, M., and Leibundgut, B., editors, *The Scientific Requirements for Extremely Large Telescopes*, volume 232 of *IAU Symposium*, pages 350–355.
- Jackson, J. D. and Fox, R. F. (1999). Classical Electrodynamics, 3rd ed. *American Journal of Physics*, 67(9):841–842.
- Jonas, J. L. and the MeerKAT Team (2016). The meerkat radio telescope. In *MeerKAT Science: On the Pathway to the SKA*, page 1. PoS.
- Keller, C. U. (2002). Instrumentation for astrophysical spectropolarimetry. In Trujillo-Bueno, J., Moreno-Insertis, F., and Sánchez, F., editors, *Astrophysical Spectropolarimetry*, pages 303–354.
- Kliger, D. S., Lewis, J. W., and Randall, C. E. (1990). *Polarized Light in Optics and Spectroscopy*. Academic Press, New York.
- Kole, M., Iacovelli, F., Mancarella, M., and Produit, N. (2023). Adding gamma-ray polarime-

- try to the multi-messenger era. Prospects of joint gravitational-wave and gamma-ray polarimetry studies. A&A, 669:A77.
- Kosenkov, I. A., Berdyugin, A. V., Piirola, V., Tsygankov, S. S., Pallé, E., Miles-Páez, P. A., and Poutanen, J. (2017). High-precision optical polarimetry of the accreting black hole V404 Cyg during the 2015 June outburst. *MNRAS*, 468(4):4362–4373.
- Kostogryz, N. M., Yakobchuk, T. M., and Berdyugina, S. V. (2015). Polarization in Exoplanetary Systems Caused by Transits, Grazing Transits, and Starspots. *ApJ*, 806(1):97.
- Landi Degl'Innocenti, E. and Landolfi, M. (2004). *Polarization in Spectral Lines*, volume 307. Springer, Dordrecht.
- Lazarian, A. and Hoang, T. (2007). Radiative torques: analytical model and basic properties. *MNRAS*, 378(3):910–946.
- Leroy, J. L. (1990). Broad-band polarization in crowded spectra. A&A, 237:237.
- Li, A. and Greenberg, J. M. (1997). A unified model of interstellar dust. *A&A*, 323:566–584. Lomb, N. R. (1976). Least-Squares Frequency Analysis of Unequally Spaced Data. *Ap&SS*, 39(2):447–462.
- Lucas, P. W., Hough, J. H., Bailey, J. A., Tamura, M., Hirst, E., and Harrison, D. (2009). Planetpol polarimetry of the exoplanet systems 55Cnc and  $\tau$ Boo. *MNRAS*, 393(1):229–244.
- Lupie, O. L. and Stockman, H. S. (1988). Calibration of the Hubble Space Telescope polarimetric modes. In Coyne, G. V., Magalhaes, A. M., Moffat, A. F., Schulte-Ladbeck, R. E., and Tapia, S., editors, *Polarized Radiation of Circumstellar Origin*, pages 705–726.
- Manset, N. and Bastien, P. (2000). Polarimetric Variations of Binary Stars. I. Numerical Simulations for Circular and Eccentric Binaries in Thomson Scattering Envelopes. *AJ*, 120(1):413–429.
- Mathis, J. S. (1986). The Alignment of Interstellar Grains. ApJ, 308:281.
- Maxwell, J. C. (1865). A Dynamical Theory of the Electromagnetic Field. *Philosophical Transactions of the Royal Society of London Series I*, 155:459–512.
- McArthur, B. E., Benedict, G. F., Barnes, R., Martioli, E., Korzennik, S., Nelan, E., and Butler, R. P. (2010). New Observational Constraints on the  $\upsilon$  Andromedae System with Data from the Hubble Space Telescope and Hobby-Eberly Telescope. ApJ, 715(2):1203–1220.
- McLean, I. S. (1979). Interpretation of the intrinsic polarization of early-type emission-line stars. *MNRAS*, 186:265–285.
- McMillan, R. S. (1976). Interstellar polarization in front of the young cluster NGC 7380. *AJ*. 81:970.
- Medhi, B. J., Maheswar, G., Pandey, J. C., Kumar, T. S., and Sagar, R. (2008). Optical polarimetric study of open clusters: distribution of interstellar matter towards NGC 654. *MNRAS*, 388(1):105–116.
- Menard, F. and Bastien, P. (1992). Linear Polarization observations of T Tauri Stars. II. A Sample of Objects Fainter than 13th Magnitude. *AJ*, 103:564.
- Minniti, D., Coyne, G. V., and Claria, J. J. (1992). Linear Polarization of Stars in Seven Matel-Poor Globular Clusters. *AJ*, 103:871.
- O'Donnell, J. E. (1994). R v-dependent Optical and Near-Ultraviolet Extinction. *ApJ*, 422:158.
- Panopoulou, G. V., Hensley, B. S., Skalidis, R., Blinov, D., and Tassis, K. (2019). Extreme starlight polarization in a region with highly polarized dust emission. *A&A*, 624:L8.

- Patat, F. and Romaniello, M. (2006). Error Analysis for Dual-Beam Optical Linear Polarimetry. *PASP*, 118(839):146–161.
- Perley, R., Napier, P., Jackson, J., Butler, B., Carlson, B., Fort, D., Dewdney, P., Clark, B., Hayward, R., Durand, S., Revnell, M., and McKinnon, M. (2009). The Expanded Very Large Array. *IEEE Proceedings*, 97(8):1448–1462.
- Piirola, V., Berdyugin, A., and Berdyugina, S. (2014). DIPOL-2: a double image high precision polarimeter. In Ramsay, S. K., McLean, I. S., and Takami, H., editors, *Ground-based and Airborne Instrumentation for Astronomy V*, volume 9147 of *Society of Photo-Optical Instrumentation Engineers (SPIE) Conference Series*, page 91478I.
- Piirola, V., Kosenkov, I. A., Berdyugin, A. V., Berdyugina, S. V., and Poutanen, J. (2021). Double Image Polarimeter—Ultra Fast: Simultaneous Three-color (BV R) Polarimeter with Electron-multiplying Charge-coupled Devices. *AJ*, 161(1):20.
- Piskorz, D., Benneke, B., Crockett, N. R., Lockwood, A. C., Blake, G. A., Barman, T. S., Bender, C. F., Carr, J. S., and Johnson, J. A. (2017). Detection of Water Vapor in the Thermal Spectrum of the Non-transiting Hot Jupiter Upsilon Andromedae b. *AJ*, 154(2):78.
- Planck Collaboration, Akrami, Y., Ashdown, M., Aumont, J., Baccigalupi, C., Ballardini, M., Banday, A. J., Barreiro, R. B., Bartolo, N., Basak, S., Benabed, K., Bernard, J. P., Bersanelli, M., Bielewicz, P., Bond, J. R., Borrill, J., Bouchet, F. R., Boulanger, F., Bracco, A., Bucher, M., Burigana, C., Calabrese, E., Cardoso, J. F., Carron, J., Chiang, H. C., Combet, C., Crill, B. P., de Bernardis, P., de Zotti, G., Delabrouille, J., Delouis, J. M., Di Valentino, E., Dickinson, C., Diego, J. M., Ducout, A., Dupac, X., Efstathiou, G., Elsner, F., Enßlin, T. A., Falgarone, E., Fantaye, Y., Ferrière, K., Finelli, F., Forastieri, F., Frailis, M., Fraisse, A. A., Franceschi, E., Frolov, A., Galeotta, S., Galli, S., Ganga, K., Génova-Santos, R. T., Ghosh, T., González-Nuevo, J., Górski, K. M., Gruppuso, A., Gudmundsson, J. E., Guillet, V., Handley, W., Hansen, F. K., Herranz, D., Huang, Z., Jaffe, A. H., Jones, W. C., Keihänen, E., Keskitalo, R., Kiiveri, K., Kim, J., Krachmalnicoff, N., Kunz, M., Kurki-Suonio, H., Lamarre, J. M., Lasenby, A., Le Jeune, M., Levrier, F., Liguori, M., Lilje, P. B., Lindholm, V., López-Caniego, M., Lubin, P. M., Ma, Y. Z., Macías-Pérez, J. F., Maggio, G., Maino, D., Mandolesi, N., Mangilli, A., Martin, P. G., Martínez-González, E., Matarrese, S., McEwen, J. D., Meinhold, P. R., Melchiorri, A., Migliaccio, M., Miville-Deschênes, M. A., Molinari, D., Moneti, A., Montier, L., Morgante, G., Natoli, P., Pagano, L., Paoletti, D., Pettorino, V., Piacentini, F., Polenta, G., Puget, J. L., Rachen, J. P., Reinecke, M., Remazeilles, M., Renzi, A., Rocha, G., Rosset, C., Roudier, G., Rubiño-Martín, J. A., Ruiz-Granados, B., Salvati, L., Sandri, M., Savelainen, M., Scott, D., Soler, J. D., Spencer, L. D., Tauber, J. A., Tavagnacco, D., Toffolatti, L., Tomasi, M., Trombetti, T., Valiviita, J., Vansyngel, F., Van Tent, B., Vielva, P., Villa, F., Vittorio, N., Wehus, I. K., Zacchei, A., and Zonca, A. (2020). Planck 2018 results. XI. Polarized dust foregrounds. A&A, 641:A11.
- Poeckert, R. and Marlborough, J. M. (1976). Intrinsic linear polarization of Be stars as a function of V sini. *ApJ*, 206:182–195.
- Poutanen, J., Veledina, A., and Beloborodov, A. M. (2023). Polarized X-Rays from Windy Accretion in Cygnus X-1. *ApJ*, 949(1):L10.
- Price-Whelan, A., Crawford, S., Sipocz, B., de Val-Borro, M., Günther, H. M., Ginsburg, A., Lim, P. L., Robitaille, T., Tollerud, E., Conseil, S., Sladen, P., Barmby, P., Vanderplas, J., Igbouma, Copin, Y., Homeier, D., Dencheva, N., Buddelmeijer, H., Jenness, T., Streicher, O., mdmueller, Shupe, D., Pérez-Suárez, D., Weaver, B. A., Cruz, K.,

- Dietrich, J., Cano Rodríguez, J. L., Kovacs, G., Muna, D., and Bakanov, A. (2018). Astropy/Astropy-V2.0-Paper: Final Draft. Zenodo.
- Quanz, S. P., Schmid, H. M., Geissler, K., Meyer, M. R., Henning, T., Brandner, W., and Wolf, S. (2011). Very Large Telescope/NACO Polarimetric Differential Imaging of HD100546—Disk Structure and Dust Grain Properties between 10 and 140 AU. *ApJ*, 738(1):23.
- Roddier, F. (1981). Atmospheric limitations to high angular resolution imaging. In Corteggiani, J. P., Gay, J., and Rabbia, Y., editors, *Scientific Importance of High Angular Resolution at Infrared and Optical Wavelengths*, pages 5–22.
- Rosu, S., Quintero, E. A., Rauw, G., and Eenens, P. (2023). New insight into the massive eccentric binary HD 165052: self-consistent orbital solution, apsidal motion, and fundamental parameters. *MNRAS*, 521(2):2988–3003.
- Rudy, R. J. and Kemp, J. C. (1976). AO Cassiopeiae: phase-locked polarization and the geometry of the gas stream. *ApJ*, 207:L125–L128.
- Russell, H. N. (1916). On the Albedo of the Planets and Their Satellites. ApJ, 43:173–196.
- Rybicki, G. B. and Lightman, A. P. (1979). Book-Review Radiative Processes in Astrophysics. *Astronomy Quarterly*, 3:199.
- Saikia, D. J. and Salter, C. J. (1988). Polarization properties of extragalactic radio sources. *ARA&A*, 26:93–144.
- Sakanoi, T., Kuhn, J., Berdyugina, S., Emilio, M., Kagitani, M., Hirahara, Y., Nakagawa, H., Kasaba, Y., Obara, T., Okano, S., Scholl, I., Berdyugin, A., and Piirola, V. (2018). Development of planets telescope and visible-infrared spectrometer for monitoring of planetary and exoplanetary atmospheres. In Marshall, H. K. and Spyromilio, J., editors, *Ground-based and Airborne Telescopes VII*, volume 10700 of *Proceedings of SPIE*, page 107004J. SPIE.
- Scargle, J. D. (1982). Studies in astronomical time series analysis. II. Statistical aspects of spectral analysis of unevenly spaced data. *ApJ*, 263:835–853.
- Schmid, H. M., Beuzit, J. L., Feldt, M., Gisler, D., Gratton, R., Henning, T., Joos, F., Kasper, M., Lenzen, R., Mouillet, D., Moutou, C., Quirrenbach, A., Stam, D. M., Thalmann, C., Tinbergen, J., Verinaud, C., Waters, R., and Wolstencroft, R. (2006). Search and investigation of extra-solar planets with polarimetry. In Aime, C. and Vakili, F., editors, IAU Colloq. 200: Direct Imaging of Exoplanets: Science & Techniques, pages 165–170
- Schmid, H. M., Gisler, D., Joos, F., Povel, H. P., Stenflo, J. O., Feldt, M., Lenzen, R., Brandner, W., Tinbergen, J., Quirrenbach, A., Stuik, R., Gratton, R., Turatto, M., and Neuhäuser, R. (2005). ZIMPOL/CHEOPS: a Polarimetric Imager for the Direct Detection of Extra-solar Planets. In Adamson, A., Aspin, C., Davis, C., and Fujiyoshi, T., editors, Astronomical Polarimetry: Current Status and Future Directions, volume 343 of Astronomical Society of the Pacific Conference Series, page 89.
- Seager, S., Whitney, B. A., and Sasselov, D. D. (2000). Photometric Light Curves and Polarization of Close-in Extrasolar Giant Planets. *ApJ*, 540(1):504–520.
- Seilmayer, M. and Ratajczak, M. (2017). A guide on spectral methods applied to discrete data in one dimension. *Journal of Applied Mathematics*, 2017:1–27.
- Serkowski, K., Mathewson, D. S., and Ford, V. L. (1975). Wavelength dependence of interstellar polarization and ratio of total to selective extinction. *ApJ*, 196:261–290.
- Shakhovskoi, N. M. (1965). Polarization in Variable Stars. II. Eclipsing Binaries. *Soviet Ast.*, 8:833.

- Shannon, C. E. (1949). Communication in the Presence of Noise. *IEEE Proceedings*, 37:10–21.
- Shurcliff, W. A. (1962). Review of Publications- Polarized Light, production and use. *JRASC*, 56:269–269.
- Simmons, J. F. L., Aspin, C., and Brown, J. C. (1982). Bias of polarimetric estimators for binary star inclinations. *MNRAS*, 198:45–57.
- Singh, S. and Pandey, J. C. (2020). Broadband Linear Polarization in the Region of the Open Star Cluster NGC 1817. *AJ*, 160(6):256.
- St. -Louis, N., Moffat, A. F. J., Drissen, L., Bastien, P., and Robert, C. (1988). Polarization Variability among Wolf-Rayet Stars. III. A New Way to Derive Mass-Loss Rates for Wolf-Rayet Stars in Binary Systems. *ApJ*, 330:286.
- Stam, D. M. and Hovenier, J. W. (2005). Errors in calculated planetary phase functions and albedos due to neglecting polarization. *A&A*, 444(1):275–286.
- Stokes, G. G. (1851). On the Composition and Resolution of Streams of Polarized Light from different Sources. *Transactions of the Cambridge Philosophical Society*, 9:399.
- Stratton, J. A. and Chu, L. J. (1941). Steady-State Solutions of Electromagnetic Field Problems. I. Forced Oscillations of a Cylindrical Conductor. *Journal of Applied Physics*, 12(3):230–235.
- Strutt, J. W. (1871). On the light from the sky, its polarization and colour. *The London, Edinburgh, and Dublin Philosophical Magazine and Journal of Science*, 41(271):107–120.
- Thomson, J. J. (1906). *Conduction of Electricity through Gases*. Cambridge University Press, Cambridge, 2nd edition.
- Tinbergen, J. (2005). Astronomical Polarimetry. Cambridge University Press, Cambridge.
- Turnshek, D. A., Bohlin, R. C., Williamson, II, R. L., Lupie, O. L., Koornneef, J., and Morgan, D. H. (1990). An Atlas of Hubble Space Telescope Photometric, Spectrophotometric, and Polarimetric Calibration Objects. *AJ*, 99:1243.
- van de Hulst, H. C. (1981). *Light Scattering by Small Particles*. Dover Publications, New York.
- VanderPlas, J. T. (2018). Understanding the Lomb-Scargle Periodogram. ApJS, 236(1):16.
- Whittet, D. C. B., Martin, P. G., Hough, J. H., Rouse, M. F., Bailey, J. A., and Axon, D. J. (1992). Systematic Variations in the Wavelength Dependence of Interstellar Linear Polarization. *ApJ*, 386:562.
- Wiktorowicz, S. (2009). Non-Detection Of Polarized, Scattered Light From The HD 189733b Hot Jupiter. In *American Astronomical Society Meeting Abstracts #213*, page 346.04.
- Wiktorowicz, S. J., Nofi, L. A., Jontof-Hutter, D., Kopparla, P., Laughlin, G. P., Hermis, N., Yung, Y. L., and Swain, M. R. (2015). A Ground-based Albedo Upper Limit for HD 189733b from Polarimetry. *ApJ*, 813(1):48.
- Wilking, B. A., Lebofsky, M. J., Martin, P. G., Rieke, G. H., and Kemp, J. C. (1980). The wavelength dependence of interstellar linear polarization. *ApJ*, 235:905–910.
- Wolinski, K. G. and Dolan, J. F. (1994). Confidence intervals for orbital parameters determined polarimetrically . *MNRAS*, 267:5–12.
- Young, M. (1984). Electromagnetic and polarization effects. In *Optics and Lasers*, volume 13 of *Springer Series in Optical Sciences*, pages 173–207. Springer.
- Young, T. (1804). The bakerian lecture: Experiments and calculations relative to physical optics. *Philosophical Transactions of the Royal Society of London*, 94:1–16.





ISBN 978-952-02-0432-7 (PRINT) ISBN 978-952-02-0433-4 (PDF) ISSN 0082-7002 (PRINT) ISSN 2343-3175 (ONLINE)